**An ultra-stable gold-coordinated protein cage displaying reversible assembly**

Ali D. Malay[1,*], Naoyuki Miyazaki[2], Artur Biela[3,4], Soumyananda Chakraborti[3], Karolina Majsterkiewicz[3,5], Izabela Stupka[3,5], Craig S. Kaplan[6], Agnieszka Kowalczyk[3,7], Bernard M. A. G. Piette[8], Georg K. A. Hochberg[9,†], Di Wu[9], Tomasz P. Wrobel[10], Adam Fineberg[9], Manish S. Kushwah[9], Mitja Kelemen[11,12], Primož Vavpetič[11], Primož Pelicon[11], Philipp Kukura[9], Justin L. P. Benesch[9], Kenji Iwasaki[2,13], Jonathan G. Heddle[1,3§]

[1]Heddle Initiative Research Unit, RIKEN, Saitama, 351-0198, Japan

[2]Laboratory of Protein Synthesis and Expression, Institute for Protein Research, Osaka University, 3-2 Yamadaoka, Suita, Osaka 565-0871, Japan

[3]Bionanoscience and Biochemistry Laboratory, Malopolska Centre of Biotechnology, Jagiellonian University, Gronostajowa 7A, 30-387 Kraków, Poland

[4] Department of Cell Biology and Imaging, Institute of Zoology and Biomedical Research, Jagiellonian University, Gronostajowa 9, 30-387 Kraków, Poland

[5]Postgraduate School of Molecular Medicine; Żwirki i Wigury 61, 02-091 Warsaw, Poland

[6]David R. Cheriton School of Computer Science, University of Waterloo, Waterloo, Ontario, Canada

[7]Faculty of Mathematics and Computer Science, Jagiellonian University, Łojasiewicza 6, 30-348 Kraków, Poland

[8]Department of Mathematical Sciences, Durham University, Stockton Road, Durham, DH1 3LE, UK

[9]Department of Chemistry, Physical & Theoretical Chemistry Laboratory, University of Oxford, South Parks Road, Oxford, OX1 3QZ, UK

[10]Institute of Nuclear Physics Polish Academy of Sciences, PL-31342 Kraków, Poland

[11]Jožef Stefan Institute, Jamova 39, SI-1000 Ljubljana, Slovenia

[12] Jožef Stefan International Postgraduate School, Jamova cesta 39, 1000 Ljubljana, Slovenia

[13] Life Science Center for Survival Dynamics, Tsukuba Advanced Research Alliance (TARA), University of Tsukuba, 1-1-1 Tennodai, Tsukuba, Ibaraki 305-8577 Japan

*Present address: Biomacromolecules Research Team, Center for Sustainable Resource Science, RIKEN

2-1 Hirosawa, Wako-shi, Saitama, 351-0198, Japan

†Present address: Department of Ecology and Evolution, University of Chicago, Chicago, IL 60637, USA

§email: jonathan.heddle@uj.edu.pl

**In nature symmetrical protein cages have evolved to fulfil diverse roles including compartmentalization and cargo delivery[1] and have inspired synthetic biologists to create novel protein assemblies via precise manipulation of protein-protein interfaces. Despite the impressive array of protein cages produced in the lab, the design of inducible assemblies remains a great challenge[2,3]. Here we demonstrate an ultra-stable artificial protein cage whose assembly/disassembly can be controlled via metal coordination at the protein-protein interfaces. The addition of a gold(I)-triphenylphosphine compound to a cysteine-substituted, 11-mer protein ring triggers supramolecular self-assembly, to generate monodisperse cage structures with an unprecedented geometry based on the Archimedean snub cube, each containing 264 protein subunits (>2 MDa). Cryo-EM confirms that the assemblies are held together via 120 S-Au$^{I}$-S staples between the protein oligomers, and exist in two alternative chiral forms. The cage displays extreme chemical and thermal stability, yet readily disassembles upon exposure to reducing agents. Mercury(II) is also found capable of promoting protein cage formation. This work establishes an approach for linking protein components into robust, higher-order structures and expands the design space available for supramolecular assemblies to include previously unexplored geometries.**

Successful strategies for designing new protein cages make use of precisely oriented oligomeric protein fusions[4] or the computational design of novel protein-protein interfaces via the

introduction of multiple hydrogen bond and hydrophobic interactions.[5] One drawback of these methods, however, is that the resulting assemblies are static; *i.e.* assembly/disassembly cannot be modulated using external stimuli, an otherwise desirable trait for smart nanomaterials. Metal-directed protein assembly presents an attractive alternative in this regard: inspired by supramolecular coordination chemistry[6], it offers the prospect for directional metal ion coordination between protein surfaces to substitute for protein-protein interactions, thus greatly simplifying the design problem[7]. Although a wide variety of inducible metal-mediated protein oligomers and arrays have successfully been generated in this manner[7-10], the creation of novel 3D cage-like assemblies remains elusive, the closest being an engineered ferritin that can recover the native cage architecture upon $Cu^{II}$ binding at interfacial sites[11].

Here we create a protein cage whose assembly and disassembly can be triggered via metal ion coordination. In our previous work on TRAP, a bacterial ring-shaped protein[12,13] amenable to genetic modification[14-16], we showed that a Cys-substituted variant could form non-native shell architectures when reacted with triphenylphosphine-derivatized gold nanoparticles, via an unknown mechanism[17,18]. We hypothesized that metal ion-thiol interactions could be responsible for the formation of precise higher-order assemblies. To explore this idea, we engineered a TRAP variant bearing a K35C, which generates 11 regularly spaced thiol groups along the outer rim of the oligomeric ring, and a R64S, which neutralizes positive charges around the central cavity of the ring to prevent non-specific interactions with anionic groups[18] ($TRAP^{CS}$; **Fig. 1a**). A minimal reaction at pH 8 containing purified $TRAP^{CS}$ plus monosulfonated chloro(triphenylphosphine)gold(I) (Au-TPPMS; **Fig. 1b**), as a source of $Au^{I}$ ions, resulted in the efficient self-assembly of monodisperse spheres ("TRAP-cage") measuring ~22 nm in diameter (**Fig. 1c-d, Extended Data Table 1**), visible within a timescale of minutes with the reaction occurring optimally at pH 7-8 (**Fig. 1e**, **Extended Data Fig. 1**). Single molecule mass photometry[19] enabled the kinetic tracking of TRAP-cage formation *in situ* after addition of Au-TPPMS (**Fig. 1e, Supplementary Movies 1-9**). In the absence of Au-TPPMS, we found a homogeneous distribution of TRAP rings (**Fig 1e: inset**). Upon addition of Au-TPPMS, partially assembled TRAP-cages appeared with an average mass of 1080 kDa,

which transitioned towards fully assembled cages (2160 kDa) with a 351 ± 66 s exponential time constant.

The structure of TRAP-cage was elucidated using cryo-EM single particle analysis (**Extended Data Figs. 2-5**). An initial map (4.7 Å) showed a cage structure that oddly lacked expected chiral features at the level of individual protein components (**Extended Data Fig. 2**). A second round of 3D classification using finer angular sampling was then carried out, which yielded two unambiguous maps at 3.7 Å displaying identical features but opposite chirality (**Fig. 1f**, **Extended Data Figs. 2, 4-5**), with the left-handed (LH) and right-handed (RH) forms found in roughly equal populations based on particle counts (46.5% and 53.5%, respectively).

The maps revealed a spherical cage with unusual architecture featuring 24 uniform rings and 6 square apertures along 3 orthogonal axes (**Fig. 1f-g**). The overall arrangement corresponds to a snub cube, an Archimedean solid with underlying octahedral (432) symmetry, and an axial twist that imparts chirality (**Fig. 1h**). Each ring occupies an equivalent position on a snub cube vertex, bounded by 5 neighbouring rings, plus a gap that defines one side of a square aperture. Crucially, all 24 rings preserved the 11-fold rotational symmetry ($C_{11}$) of native TRAP protein (**Fig. 1i**). Refinement of $TRAP^{CS}$ models against each map produced excellent results (**Extended Data Table 2**). Overall, each chiral assembly is composed of 264 identical $TRAP^{CS}$ subunits (**Fig. 1j**).

Closer examination showed the ring densities to be interconnected via staple-like bridges, with two staples between each pair of neighbouring rings, totalling 120 staples per cage. In the refined models, 10 $Cys^{35}$ side chains of each $TRAP^{CS}$ ring align with the staple positions, while the unlinked side chain of the $11^{th}$ subunit points toward the 4-fold aperture (**Fig. 1i, Fig. 2a**). An enlargement at the midpoint of each staple density was observed, interpreted as an $Au^{I}$ ion coordinated between the two proximal thiol ligands, with the preferred linear geometry (**Fig. 2a**)[20]. No other ring-ring interactions were observed, aside from possible hydrogen bonding between $Asn^{18}$ and $Asp^{37}$ side chains.

The presence of gold in the final structures was measured via electrothermal atomic absorption spectroscopy (ETAAS; **Extended Data Table 3**), to be 112 ± 8 Au per assembly,

in close agreement with the predicted value of 120. The presence of gold was corroborated by mass spectrometry (MS), which produced peaks that suggest stable S-$Au^{I}$-S linkages (**Fig. 2b-d**), proton-induced X-ray emission (PIXE) and X-ray photoelectron spectroscopy (XPS), whereas Raman spectroscopy showed no evidence of direct disulphide linkages (**Extended Data Fig. 6**). The interaction between $Au^{I}$ and $Cys^{35}$ are expected to proceed via successive ligand displacement events involving Au-TPPMS, in agreement with $Au^{I}$-phosphine ligand exchange hypotheses[21,22] .

The metal-directed protein assembly strategy predicts that a supramolecular complex of desired geometry can be generated by matching the inherent symmetry of a protein oligomer with the coordination geometry of an interacting metal ion[7]. To test this hypothesis in our context, we probed additional thiophilic transition metal ions ($Au^{III}$, $Cu^{I}$, $Hg^{II}$, $Zn^{II}$) for their ability to induce cage assembly upon reaction with $TRAP^{CS}$ (**Fig. 2e-f**, **Extended Data Fig. 7a-c**). Whereas addition of $Au^{III}$, $Cu^{I}$ and $Zn^{II}$ showed little or no evidence of cage structures, $Hg^{II}$ triggered the formation of uniform cages that were indistinguishable from the gold-derived structures, consistent with the linear 2-coordinate geometry of mercury(II).

To test the robustness of the TRAP-cage architecture, the placement of thiol groups in the TRAP ring was varied by generating additional surface mutants, D15C and S33C. TRAP bearing S33C, but not D15C, could assemble into cages in the presence of Au-TPPMS, underscoring the importance of secondary interactions in influencing resultant architectures (**Extended Data Fig. 7d-f**).

The stability of TRAP-cage was measured over a range of conditions (**Fig. 3a-e, Extended Data Fig. 8**). Remarkably high stability was observed upon exposure to high temperatures, chaotropic agents, and a wide range of pH conditions, consistent with the stabilizing effect of metal coordination[23,24]. Despite extreme stability, the cages were fully reversible, breaking apart in response to millimolar levels of reducing agents, likely via ligand displacement mechanisms[21]. We also observed that the reaction of $TRAP^{CS}$ with triphenylphosphine-derivatized gold clusters produced a cage with a similar structure and stability (**Extended Data Figs. 9-10**).

From a geometrical perspective the TRAP-cage architecture presents an apparent paradox, given that $C_{11}$-symmetric polygons (hendecagons) are excluded from assembling into regular convex polyhedra (apart from prisms or antiprisms)[25]. To understand this, it is helpful to consider the geometric dual of the snub cube, the pentagonal icositetrahedron (PI) polyhedron with 24 identical non-regular pentagonal faces, arranged with octahedral symmetry. We find that a regular hendecagon can be inscribed in each face so that five of its edges nearly perfectly coincide with that of the irregular pentagon (**Fig. 4a**), implying a solid formed from 24 hendecagons, 56 triangles and 6 squares, which is mathematically impossible but plausibly constructible as a physical object. To understand this geometry further, we modelled 24 copies of $TRAP^{CS}$ oligomers as 11-pointed rings and optimized their positions in space to converge at a distance between two neighbouring points of 4.7 Å (the theoretical distance between two Cys-sulphur ligands in a S-$Au^{I}$-S linear complex). This simulation produced an arrangement reminiscent of the TRAP-cage architecture (**Fig. 4b-c**); strikingly, the optimised S-to-S distances converged to the target with vanishingly small error, well within the physical tolerances required to form uniform protein cages from $C_{11}$ symmetric elements.

Our study supports the finding that a tiny number of mutations can lead to profound changes in protein structural complexity via spontaneous self-assembly[26,27]. Intriguingly, the architecture described by TRAP-cage has, to our knowledge, never been observed in nature, although a similar arrangement of 11-pointed stars appears in Islamic art, in the Court of the Lions at the Alhambra[28]. Furthermore, our results suggest a possible avenue for building large capsid-like proteins using homomeric components. Viruses have achieved this by exploiting quasi-equivalent icosahedral symmetries to build shells of >60 subunits[29], but this poses an immense challenge for computationally designed cage systems, as it requires controlled switching between different oligomeric forms[30]. In contrast, TRAP-cage is a large, shell structure built from a single type of protein homo-oligomer, something that has only rarely been reported[27]. The general stability of TRAP-cage and its controllable disassembly hints at potential applications as an intracellular delivery agent. We suggest, finally, that beyond the unusual architecture embodied by TRAP-cage there exists an entire domain of unexplored

"paradoxical geometries" (**Fig. 4d-f**) that could be constructed using proteins or other biological molecules with potentially unique properties.

**Acknowledgements**

We thank M. Michalak and R. Pałka for initial TRAP proteins production , M. Kobiałka for TEM imaging and A. Telk and D. Dudek-Adamska for ETAAS experiments and evaluation (with financial support no.POIG.02.02.00-12-023/08). This work was performed in part under the International Cooperative Research Program of the Institute for Protein Research, Osaka University CEMCR-17-05. ADM and JGH were funded by Riken Initiative Research Funding awarded to JGH. ADM was supported by a Kakenhi Grant-In-Aid for Challenging Exploratory Research (JSPS), No. 2556023, JGH, AB and KM were funded by the National Science Centre (NCN, Poland) grant No.2016/20/W/NZ1/00095 (Symfonia-4). Raman spectroscopy experiments were performed under project No. MRPO.05.01.00-12-013/15. TPW was supported under grant No. Homing/2016-2/20. AF, MSK and PK were supported by a ERC starting investigator grant (337757). KI was supported by the Platform Project for Supporting Drug Discovery and Life Science Research (Basis for Supporting Innovative Drug Discovery and Life Science Research) from the Japan Agency for Medical Research and Development (AMED). Work at JSI was supported by the Slovenian research agency grants No. P1-0112, I0-0005, J7-9398 and EU projects No. 227012 “SPIRIT”, No. 824096 “RADIATE”.

**Author Contributions** ADM designed experiments, produced the protein cage, wrote the manuscript and carried out other experiments not listed. JGH designed experiments, carried out TEM and wrote the manuscript. CSK produced mathematical models of the TRAP-cage**.** AK and BMAGP wrote the algorithm to predict paradoxical cage structures, AB and ADM built the atomic models. NM and KI carried out cryo-EM experiments. GKAH, DW and JLPB carried out mass spectrometry experiments. TPW carried out Raman and XPS spectroscopy experiments. PP, PV and MK executed micro-PIXE analysis. SC and KM produced the protein cage, carried out stability tests and TEM sample preparation. IS carried out protein production

and purification, DLS measurements and preparation of samples for TEM and SC carried out TEM. All authors contributed to writing the manuscript.

**Competing Interests**: Authors ADM and JGH are named as inventors on a patent application related to the use of gold to cross-link cysteine residues aimed at protein assembly construction.

**REFERENCES**


1 Aumiller, W. M., Uchida, M. & Douglas, T. Protein cage assembly across multiple length scales. *Chem. Soc. Rev.* **47**, 3433-3469 (2018).

2 Bale, J. B. *et al.* Accurate design of megadalton-scale two-component icosahedral protein complexes. *Science* **353**, 389-394 (2016).

3 Yeates, T. O. Geometric principles for designing highly symmetric self-assembling protein nanomaterials. *Annu. Rev. Biophys.* **46**, 23-42 (2017).

4 Padilla, J. E., Colovos, C. & Yeates, T. O. Nanohedra: Using symmetry to design self assembling protein cages, layers, crystals, and filaments. *Proc. Natl Acad. Sci. USA* **98**, 2217-2221 (2001).

5 King, N. P. *et al.* Computational design of self-assembling protein nanomaterials with atomic level accuracy. *Science* **336**, 1171-1174 (2012).

6 Holliday, B. J. & Mirkin, C. A. Strategies for the construction of supramolecular compounds through coordination chemistry. *Angew. Chem. Int. Edit.* **40**, 2022-2043 (2001).

7 Salgado, E. N., Radford, R. J. & Tezcan, F. A. Metal-directed protein self-assembly. *Acc. Chem. Res.* **43**, 661-672 (2010).

8 Brodin, J. D. *et al.* Metal-directed, chemically tunable assembly of one-, two- and three-dimensional crystalline protein arrays. *Nat. Chem.* **4**, 375-382 (2012).

9 Der, B. S. *et al.* Metal-mediated affinity and orientation specificity in a computationally designed protein homodimer. *J. Am. Chem. Soc.* **134**, 375-385 (2011).

10 Zhang, W. *et al.* Self-assembly of glutathione S-transferase into nanowires. *Nanoscale* **4**, 5847-5851 (2012).

11 Huard, D. J. E., Kane, K. M. & Tezcan, F. A. Re-engineering protein interfaces yields copper-inducible ferritin cage assembly. *Nat. Chem. Biol.* **9**, 169 (2013).

12 Antson, A. A. *et al.* The structure of trp RNA-binding attenuation protein. *Nature* **374**, 693-700 (1995).

13 Chen, X. *et al.* Regulatory features of the trp operon and the crystal structure of the trp RNA-binding attenuation protein from Bacillus stearothermophilus. *J. Mol. Biol.* **289**, 1003-1016 (1999).

14 Heddle, J. G., Yokoyama, T., Yamashita, I., Park, S.-Y. & Tame, J. R. H. Rounding up: Engineering 12-membered rings from the cyclic 11-mer TRAP. *Structure* **14**, 925-933 (2006).

15 Heddle, J. G. *et al.* Using the ring-shaped protein TRAP to capture and confine gold nanodots on a surface. *Small* **3**, 1950-1956 (2007).

16 Miranda, F. F. *et al.* A Self-Assembled Protein Nanotube with High Aspect Ratio. *Small* **5**, 2077-2084 (2009).

17 Malay, A. D. *et al.* Gold Nanoparticle-Induced Formation of Artificial Protein Capsids. *Nano Lett.* **12**, 2056-2059 (2012).

18 Imamura, M. *et al.* Probing structural dynamics of an artificial protein cage using high-speed atomic force microscopy. *Nano Lett.* **15**, 1331-1335 (2015).

19 Young, G. *et al.* Quantitative mass imaging of single biological macromolecules. *Science* **360**, 423-427 (2018).

20 Häkkinen, H. The gold-sulfur interface at the nanoscale. *Nat. Chem.* **4**, 443-455 (2012).

21 Bhabak, K. P., Bhuyan, B. J. & Mugesh, G. Bioinorganic and medicinal chemistry: aspects of gold(I)-protein complexes. *Dalton Trans.* **40**, 2099-2111 (2011).

22 Urig, S. *et al.* Undressing of phosphine gold(I) complexes as irreversible inhibitors of human disulfide reductases. *Angew. Chem. Int. Ed. Engl.* **45**, 1881-1886 (2006).

23 Arnold, F. H. & Zhang, J. H. Metal-mediated protein stabilization. *Trends Biotechnol.* **12**, 189-192 (1994).

24 Brodin, J. D., Carr, J. R., Sontz, P. A. & Tezcan, F. A. Exceptionally stable, redox-active supramolecular protein assemblies with emergent properties. *Proc. Natl. Acad. Sci. USA* **111**, 2897-2902 (2014).

25 Grünbaum, B. & Johnson, N. W. The faces of a regular‐faced polyhedron. *J. London Math. Soc.* **40**, 577-586 (1965).

26 Garcia-Seisdedos, H., Empereur-Mot, C., Elad, N. & Levy, E. D. Proteins evolve on the edge of supramolecular self-assembly. *Nature* **548**, 244-247 (2017).

27 Sasaki, E. *et al.* Structure and assembly of scalable porous protein cages. *Nature Communications* **8** (2017).

28 Redondo, A. & Huylebrouck, D. in *Bridges Finland Conference Proceedings.* 497-500 (2016).

29 Caspar, D. L. D. & Klug, A. Physical principles in construction of regular viruses. *Cold Spring Harb. Symp. Quant. Biol.* **27**, 1-24 (1962).

30 Prasad, B. V. & Schmid, M. F. Principles of virus structural organization. *Adv. Exp. Med. Biol.* **726**, 17-47 (2012).

**Figures**

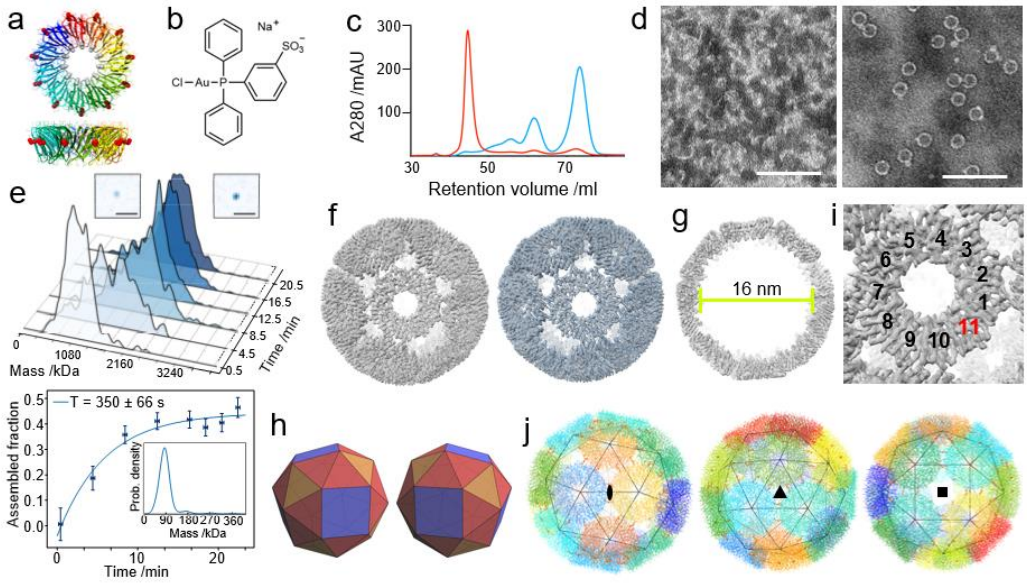


**Figure 1. Formation of TRAP-cage. a**, Structure of the TRAP$^{CS}$ building block, shown in two orthogonal views (based on PDB 4V4F). The substituted residues Cys$^{35}$ and Ser$^{64}$ are modelled as red and grey spheres, respectively. **b**, Chemical structure of Au-TPPMS. **c**, Results of size exclusion chromatography (SEC), with 1 mM (monomer concentration) TRAP$^{CS}$ before (blue) and 3 days after (red) reaction with Au-TPPMS. Unreacted TRAP$^{CS}$ shows heterogeneous size distribution, with a major peak corresponding to lower molecular weight TRAP ring assemblies and a smaller peak corresponding to larger aggregates likely resulting from disulphide bond formation. SEC is representative of two independent experiments giving similar results. **d**, TEM images of unreacted TRAP$^{CS}$ (left) showing heterogeneous aggregates with no evidence of cage structures and (right) cages purified via SEC after mixing 1 mM each of TRAP$^{CS}$ and Au-TPPMS. Scale bars = 100 nm. TEM was repeated twice, giving similar results. **e,** Top: Monitoring TRAP-cage assembly with single molecule mass photometry. Insets: representative single particle images of partially and fully assembled cages. Scale bar: 1 µm. Bottom: Extracted assembly kinetics. Horizontal error bars: 15 s, as dictated by the length of a single measurement. Vertical error bars: standard error on the area of Gaussian fit, calculated from the covariance matrix of the fit parameters. Inset: Results for TRAP$^{CS}$ without addition of Au-TPPMS exhibiting mostly monomeric TRAP (11mer) rings (90 kDa), with weak signatures of

small oligomeric assemblies thereof. The experiment was run twice, giving similar results. **f**, Cryo-EM density maps of the LH and RH forms of TRAP-cage, refined to 3.7 Å resolution. **g**, Cutaway view of the LH map, showing a hollow interior with an internal diameter of 16 nm. **h**, Snub cube, showing LH and RH chiral forms, consisting of 32 regular triangles and 6 square faces. The 4-, 3- and 2-fold rotational axes are represented in blue, yellow, and red, respectively. **i,** Close-up of the LH map showing 11-fold rotational symmetry of ring elements and prominent density bridges connecting adjacent rings. Positions 1-10 make contacts with neighbouring rings while position 11 is unattached and defines the side of a square aperture. **j,** Refined LH cage model, consisting of 24 $TRAP^{CS}$ rings, with each ring positioned on the vertex of a snub cube (wire model). Three views are indicated, centred on the 2-, 3-, and 4-fold symmetry axes.

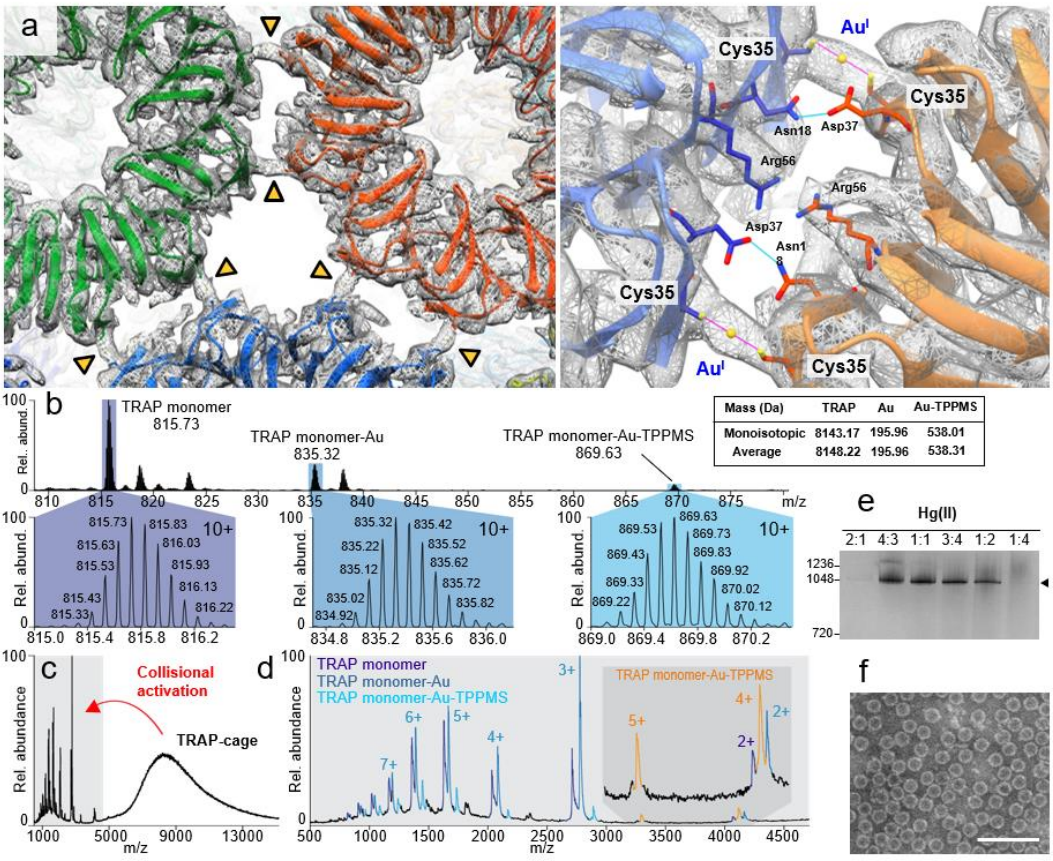


**Figure 2. TRAP-cage is held together via Cys-Au$^{I}$-Cys coordination. a,** Left, view of LH TRAP-cage model and map, with arrows indicating density bridges connecting neighbouring TRAP$^{CS}$ rings. Right, close-up of the interface between two TRAP$^{CS}$ rings in the LH cage, where individual Au$^{I}$ ions are held in linear coordination between two Cys$^{35}$ side chains from the neighbouring rings (magenta lines). No other intermolecular interactions are apparent between adjacent rings, apart from possible hydrogen bonding between Asn$^{18}$ and Asp$^{37}$ sidechains (light blue lines). **b,** Denaturing LC-MS data reveal three forms of TRAP monomer: unliganded protein (dark blue), monomer bound to a single gold atom (blue), and monomer bound to a gold atom and TPPMS ligand (light blue). Only 10+ charge states are shown for clarity, and magnifications of the different peaks allows accurate mass determination for unambiguous assignment. The other, minor peaks correspond to salt adducts and/or other charge states. Inset table: list of TRAP masses, and the mass additions expected due to the different modifications. These correspond well to the masses measured, taking into account the 10 protons responsible for the 10+ charge state. **c,** Native MS of intact TRAP-cages performed

at high collisional activation reveals a broad, unresolved region of signal at high *m*/*z*, and a series of peaks at low *m*/*z*, corresponding to dissociation of intact cages and release of cage fragments. For **b** and **c**, experiments were each repeated independently at least three times with representative results shown. **d,** Expansion of low-*m*/*z* region in **c**, showing assignment of the various charge state series. Monomeric TRAP, in both modified and unmodified forms (blues, same colouring as **b**), are the major fragments observed. Inset: notably, peaks that can be assigned unambiguously to a TRAP dimer containing a single gold atom are observed, validating the TRAP-$Au^{I}$-TRAP linkage hypothesis. **e**, $Hg(NO_3)_2$ also facilitates cage formation, as shown by native PAGE. Arrowhead indicates position of TRAP-cage formed with Au-TPPMS. Molar ratios of $TRAP^{CS}$ monomer:$Hg^{II}$ are shown on top. Apparent molecular weights are indicated. Gel is representative of two independent experiments, each giving similar results. **f**, TEM image showing products of $TRAP^{CS}$ + $Hg(NO_3)_2$ reaction, without additional purification. TEM is representative of three independent experiments, each giving similar results. Scale bar = 100 nm**.** For gel source data, see Supplementary Figure 1.

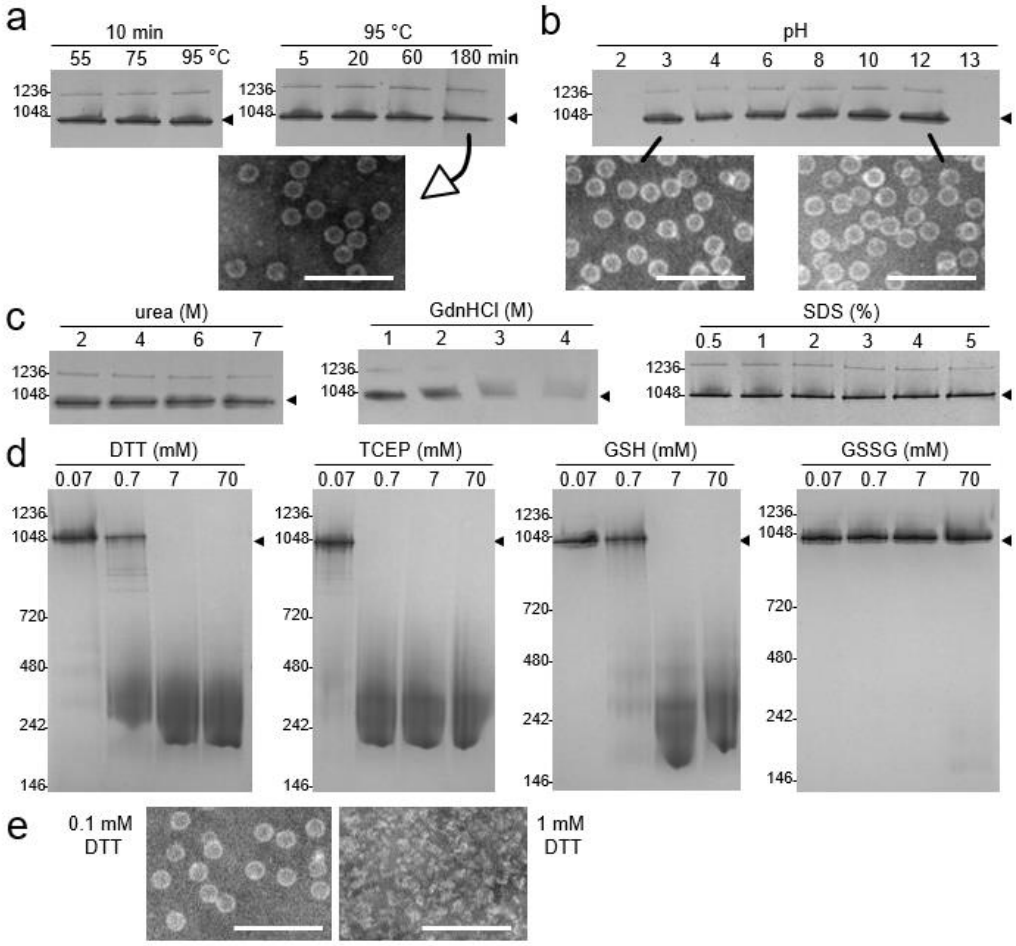


**Figure 3. Extreme stability and controllable disassembly of TRAP-cage.**

**a**, Thermal stability of TRAP-cage. Native PAGE shows preservation of structural integrity at indicated incubation times and temperatures. The TEM image shows results after incubation at 95 °C for 180 min. **b**, Stability as a function of pH. TRAP-cage samples were incubated overnight in buffer at pH 2-13. No visible loss of structure was detected from pH 3-12 using native PAGE. TEM images show the results after incubation at pH 3 and 12. **c**, Effects of urea (2-7 M), guanidine hydrochloride (1-4 M) and SDS (0.5-5%). **d**, Disassembly of TRAP-cage in the presence of reducing agents: DTT, TCEP, and reduced/oxidized glutathione (GSH and GSSG, respectively) at the indicated concentrations. All gels are representative of at least two independent experiments, each giving similar results. **e**, TEM images show structural integrity of TRAP-cage after treatment with 0.1 mM and 1 mM DTT. For all TEM, images are

representative of at least two independent experiments, each giving similar results and . Scale bars = 100 nm. For gels,  arrowheads indicate position of TRAP-cage and apparent molecular weights in kDa are indicated. For gel source data, see Supplementary Figure 1.

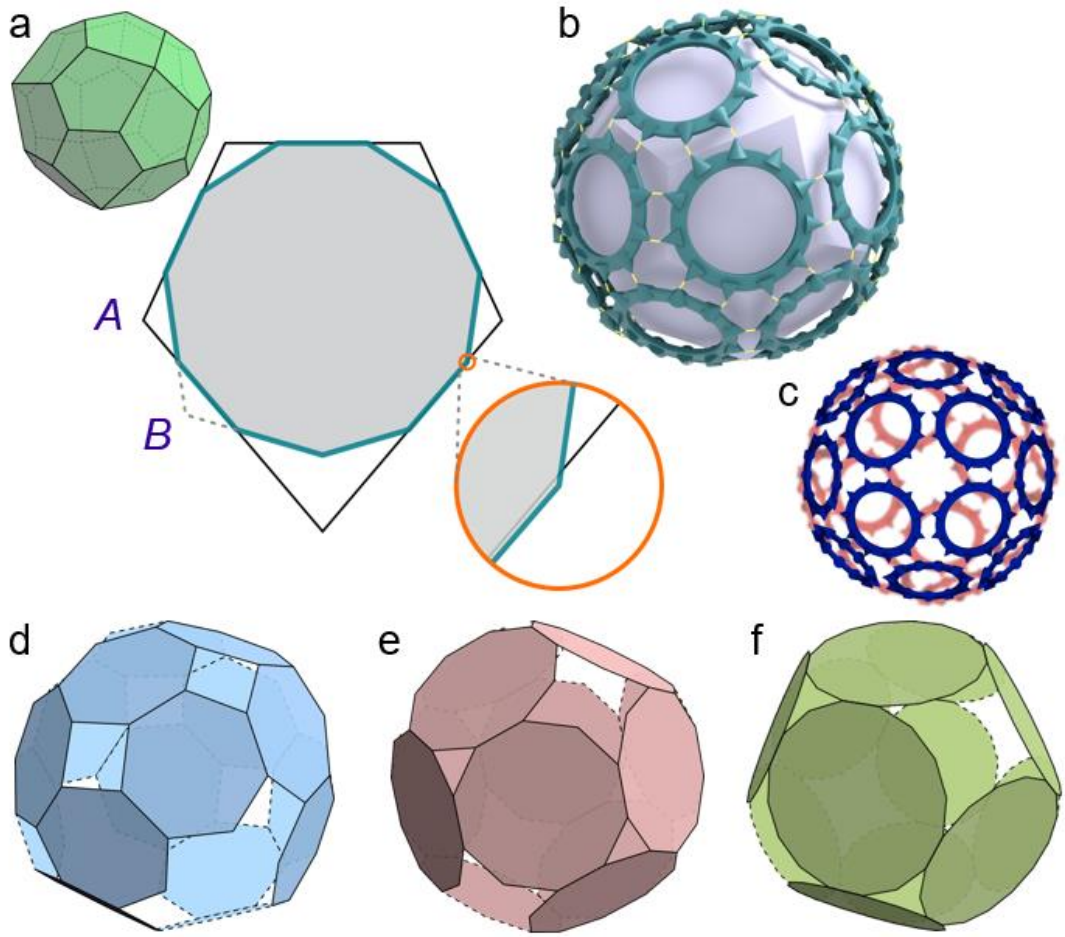


**Figure 4: Unusual geometry of TRAP-cage. a**, Top, pentagonal icositetrahedron (PI), with 24 non-regular pentagonal faces. Bottom, a regular hendecagon can be placed at each PI face such that 5 of the hendecagon's edges align almost perfectly with those of the PI. A close-up view shows that some hendecagon vertices lie very slightly outside of the PI face (others lie slightly inside). The near-coincidence arises because the obtuse angle $A \approx 114.81°$ of the PI face is almost equal to $B \approx 114.55°$ between non-consecutive hendecagon edges. **b**, Graphical representation showing the optimization of distances linking 24 regular 11-pointed rings (in yellow). Translated to the scale of TRAP-cage, the results converge almost exactly to the ideal sulphur-to-sulphur distance of 4.7 Å. **c**, The 24 rings can be divided into two groups of 12, centred on opposite ends of a fourfold rotational axis of the TRAP-cage. One such group is shown in **c**, coloured blue with the other group shown in red, faded in the background. Like the

PI, the TRAP-cage as a whole is chiral. **d-f**, Examples of paradoxical cages that can be constructed from 7, 10 and 16-sided polygons. Deviations from ideality are expressed as relative deformation, the relative difference between the largest and smallest edge lengths ($rd_l$) or angles ($rd_a$). For comparison, $rd_l$ and $rd_a$ for TRAP-cage are 0.50% and 0.27% respectively. **d**, A cage made out of 16 heptagons with 222 dihedral symmetry, derived by minimizing the energy of a mechanical model. $rd_l$ = 0.51% $rd_a$ = 0.47%. **e**, A cage made out 12 decagons obtained by dressing a cuboctahedron; $rd_l$ = 0.00% $rd_a$ = 0.51%. **f**, A cage made out of 12 hexadecagons obtained by dressing a cuboctahedron; $rd_l$ = 0.00% $rd_a$ = 0.64%.

## METHODS

*Gold compounds*

Chloro[diphenyl(3-sulfonatophenyl)phosphine]gold(I) sodium salt hydrate (Au-TPPMS) was purchased from STREM Chemicals UK and reconstituted in water to 5 mM stock concentration or in 50 mM Tris-HCl, pH 7.9, 0.15 M NaCl to 10 mM stock concentration prior to use. The gold nanoparticle (GNP) used was a diphenyl(m-sulfonatophenyl)phosphine-gold nanocluster with a 1-3 nm core diameter (MDL number MFCD17018839) from STREM Chemicals UK.

*Protein expression and purification*

In a typical purification, *E. coli* BL21(DE3) cells (Novagen) transformed with pET21b plasmid harboring the $TRAP^{CS}$ gene or pET151/D-TOPO for genes encoding TRAPs having alternative cysteines S33C and D15C, were grown at 37 °C with shaking in 3 L of LB medium with 100 μg/ml ampicillin until $OD_{600}$ = 0.6, induced with 0.5 mM IPTG then further shaken for 4-5 h. Cells were harvested by centrifugation and the pellet kept at -80 °C until use. Cells were lysed by sonication at 4 °C in 50 ml of 50 mM Tris-HCl, pH 7.9 or 8.5, 0.05 M NaCl in presence of proteinase inhibitors (Thermo Scientific) and presence or absence of 2 mM DTT, and lysates were centrifuged at 66,063 *g* for 0.5 h at 4 °C. The supernatant fraction was heated at 70 °C for 10 min, cooled to 4 °C, and centrifuged again at 66,063 *g* for 0.5 h at 4 °C. The supernatant fraction was purified by ion exchange chromatography on an ÄKTA purifier (GE Healthcare Life Sciences) using 4 × 5 ml HiTrap QFF columns with binding in 50 mM Tris-HCl, pH 7.9 or 8.5, 0.05 M NaCl, +/-2 mM DTT buffer and eluting with a 0.05 -1 M NaCl gradient. Fractions containing TRAP were pooled and concentrated using Amicon Ultra 10 kDa MWCO centrifugal filter units (Millipore) and the sample subjected to size exclusion chromatography on a HiLoad 26/600 Superdex 200pg column in 50 mM Tris-HCl, pH 7.9, 0.15 M NaCl ("cage buffer") at room temperature. Protein concentrations were calculated using the BCA protein assay kit (Pierce Biotechnology).

*Cage assembly*

Formation of TRAP-cage was carried out by mixing purified $TRAP^{CS}$ and Au-TPPMS in aqueous solution. The typical "standard cage formation conditions" consisted of equimolar amounts of $TRAP^{CS}$ monomer and Au-TPPMS in cage buffer. The exact concentrations of reactants were tailored for each reaction but were typically as follows: 1 mM $TRAP^{CS}$ (8.3 mg/ml) and 1 mM Au-TPPMS. Reactions were incubated for at least 3 days at room temperature, reaction times of up to three months were also found to give similar results. Formation of TRAP-cage was confirmed using TEM and native PAGE. Any precipitated material (aggregated protein, present in older samples) was removed by centrifugation at 12 045 *g* for 5 min, and TRAP-cage was purified by size exclusion chromatography on either Superose 6 Increase 10/300 GL or HiPrep 16/60 Sephacryl S-500 HR columns or HiLoad 16/600 Superdex 200pg column (GE Healthcare). Fractions containing the cage protein were pooled, concentrated using Amicon Ultra 0.5 100 kDa MWCO centrifugal filter units, and protein concentration was measured using the BCA protein assay (Pierce Biotechnology). Yield was calculated by passing $TRAP^{CS}$ after the cage-forming reaction with Au-TPPMS, down a Superose 6 Increase column (GE Healthcare). Fractions containing TRAP-cage were collected and purity confirmed by native PAGE. Concentration of purified cage was determined by measuring absorption at 280 nm compared to total protein concentration in the starting solution.

For formation of TRAP-cage using gold nanoparticles (GNP) in place of Au-TPPMS, conditions used were similar to the conditions described above: in brief, purified $TRAP^{CS}$ (final concentration of ~ 500 µM TRAP monomer) was mixed with GNP (final concentration ~ 500 µM) at room temperature in buffer containing 20 mM Tris-HCl, pH 8.0 and 0.15 M NaCl.

For testing the ability of other metals to support cage formation, mercury(II) nitrate (Merck), copper(I) iodide (Sigma-Aldrich), zinc chloride (VWR Chemicals) and gold(III) chloride trihydrate (Sigma-Aldrich) were reconstituted in cage buffer to 5 mM stock concentration prior to use. $TRAP^{CS}$ samples (0.8 mg/ml final concentration) were incubated for 3 days with varying metal ion concentrations. Results were monitored using native PAGE. Cages made using mercury(II) nitrate were imaged in TEM without further purification.

For testing the effect of pH on cage assembly, Au-TPPMS stocks were prepared as described above. Samples were incubated for 3 days with varying concentrations of Au(I) ions concentration in 50 mM sodium acetate at pH 5.0, 50 mM potassium phosphate at pH 6.0 or 7.0, 50 mM Tris-HCl at pH 8.0, 50 mM glycine-NaOH at pH 9.0.

For testing TRAP-cage formation at different pHs at different time points, reactions were carried out as described above for testing pH at a single time point with samples being removed at the indicated times before being mixed with 4x Native-PAGE sample buffer.

*Cage stability*

All agents used for cage stability tests (DTT, TCEP, GSH, GSSG, SDS, Gdn-HCl, Urea) were reconstituted in water or cage buffer and pH adjusted when needed. Buffers used for pH stability tests were: 50 mM glycine-HCl at pH 2.0 or 3.0, 50 mM sodium acetate at pH 4.0, 50 mM potassium phosphate at pH 6.0, 50 mM Tris-HCl at pH 8.0, 50 mM glycine-NaOH at pH 10, 50 mM potassium phosphate at pH 12, 50 mM potassium chloride-NaOH at pH 13. Each sample was briefly centrifuged in a desk-top centrifuge and a portion of supernatant removed and mixed with 4x native PAGE sample buffer and subjected to blue native PAGE.

*Dynamic light scattering*

Dynamic light scattering (DLS) was carried out using a Zetasizer Nano ZS (Malvern). TRAP-cage samples were diluted to 0.2 – 0.4 µM cage in 50 mM Tris-HCl, 150 mM NaCl, pH 7.9 and centrifuged for 2 min. at 12045 g. 50 µl of each sample were analysed in a quartz cuvette (ZEN 2112) and preincubated for 120 s at 25 °C. The samples were measured with standard settings for 50 mM Tris-HCl, 150 mM NaCl buffer. Results were given as volume distributions. Three TRAP-cage samples were measured with each measurement being repeated at least three times. All measurements gave highly similar results.

*Surface charge models*

Surface charges of proteins $TRAP^{CS}$ (based on pdb 4v4f[1]) and -21GFP (based on pdb 1gfl[2]) were calculated using Coulombic Surface software in USCF Chimera with settings of dielectric constant 4.0, distance from surface 1.4 and distance-dependent dielectric. The mutations in $TRAP^{CS}$, namely R64S and K35C were placed into the structure using USCF Chimera

*Single molecule mass photometry*

Experimental Setup: The experimental setup is identical to that described in Young et al.[3] except for the use of a 633 nm laser diode (Lasertack). Briefly, the collimated laser output is passed through two acousto-optic deflectors (AODs; AA Opto Electronic, DT SXY-400) mounted orthogonally to each other. The beam deflection is imaged into the back focal plane of a microscope objective (Olympus, 1.45 NA, 60×) by a 4f telecentric lens system after first passing through a polarising beam splitter (PBS) and a quarter-wave-plate (QWP). The light reflected at the glass-water interface together with that backscattered by the sample is collected by the objective, and this is separated from the incident light by the combination of the PBS and QWP. The reflected light is then selectively attenuated with respect to the scattering signal, by reimaging the back focal place of the microscope objective onto a partially reflective mirror, as described in Cole, et al.[4] The sample is then imaged onto a CMOS camera (Point Grey GS3-U3-23S6M-C) with 291.7× magnification, giving a pixel size of 20 nm/pixel. The focus position is maintained throughout the experiment by an active feedback loop using a total internally reflected beam.

Data Acquisition and Analysis: The camera was run at 1 kHz and the recorded images were time-averaged 2-fold and pixel-binned 5x5 before saving. This gives an effective frame rate of 500 Hz and pixel size of 100 nm. At this imaging speed, the sensitivity was insufficient to detect individual 90 kDa subunits, producing a cut off at 200 kDa for the smallest detectable objects. For control experiments to detect individual TRAP rings, data was recorded in a similar manner but was time averaged down to 10 Hz in order to increase sensitivity and detect the 90 kDa

rings. In order to reduce the number of binding events per second, the control data was measured at 100 nM.

A sample of $TRAP^{CS}$ protein in cage buffer and Au-TPPMS were incubated at room temperature in a 1:1 ratio at 100 µM each. At various time points beginning 30 s after mixing the two components, 5 µL of the mixture was diluted to 10 µM and immediately added to a well of a silicon gasket (3 mm diameter, 1 mm thickness) fixed to a microscope coverslip (#1.5, 24 mm x 52 mm, Menzel Glazer) already containing 15 uL of cage buffer and mixed with the volume of the 5 µl micro-pipette. 15 s after addition of sample to the well, the acquisition software was triggered and the sample was measured for 30s.

Image analysis was performed using the method described in Young et al.[3] to extract the masses of the observed particles. Kernel density estimates for each time point were generated using a Gaussian kernel with bandwidth of 40 kDa. To determine the proportion of formed cage with time, a Gaussian constrained to the expected mass of the cage and width for a single species of that mass ($\mu$ = 2160 kDa, $\sigma$ = 110 kDa) was fit to a normalised histogram of each time point and the area taken. The $\sigma$ value was chosen through extrapolation of values for known calibrants.

The resulting plot of proportion of cage vs. time was fit to a global association rate fit:

$$f(x) = k(1 - e^{-x/\tau})$$

where k is the maximum proportion of cage, $\tau$ is the formation time.

*3D reconstruction of initial cryo-EM structure of TRAP-cage*

A few microliters of purified TRAP-cage formed using GNPs in 20 mM Tris-HCl, pH 8.0, 0.15 M NaCl were applied onto glow-discharged C-flat grids (1 µm hole, 1 µm space, 400 mesh copper grids) in the humidity-controlled chamber of an EM GP (Leica Microsystems, Vienna, Austria) followed by blotting and plunge freezing. Cryo-EM images were collected at liquid nitrogen temperature on a JEM-2200FS transmission electron microscope (JEOL, Tokyo, Japan) operated at 200 kV using a CT3500 cryo-transfer holder (Gatan, Pleasanton, CA). Images were recorded using a K2 summit direct electron camera (Gatan, Pleasanton, CA) using

super-resolution counting mode. A nominal magnification of 20,000× reading in the electron microscope used for image recording corresponds to a calibrated super resolution pixel size of 1.01 Å per pixel on the specimen. Dose fractionation mode was used, setting frame exposure time to 0.2 s and total exposure time to 5 s. The dose rate on the camera was set to be less than 2 counts per sub-pixel per second. Stacked images obtained by dose fractionation mode underwent motion correction using software as described by Li et al.[5] All of the 25 frames in each stacked image were used to calculate a sum of frames after motion correction. Each summed image was 2×2 binned, which were used for the following image processing. The phase of the cryo-EM images was corrected using ctfDisplay and mrcImageCTFCompensation implemented under EOS.[6] Boxing 4472 particles from the phase-corrected images was done using EMAN2.[7] A first 3-D model was obtained at 18 Å (fsc = 0.5) using EMAN1.9.[8] This was used as a reference model for the image analysis by RELION1.3 and 1.4.[9] The 3D map of 16.5 Å resolution obtained without any symmetrical operation after *3D auto-refine* of RELION, was used for the following high resolution work as an initial model.

*Cryo-EM single particle reconstruction of TRAP-cage formed using GNPs at higher resolution*

Purified sample formed using GNPs (3 µl of 0.13 mg/ml) was applied to glow-discharged holey carbon grids (Quantifoil R 1.2/1.3, Mo 200 mesh) with a thin amorphous carbon film of ~10 nm thickness over the holes and incubated for 30 s at 4 °C and 100% humidity. Grids were then blotted for 3.0 s and plunged into liquid ethane using a Vitrobot Mark IV (FEI). Data were recorded semi-automatically using the EPU software on a transmission electron cryo-microscope (FEI Titan Krios) operated at an accelerating voltage of 300 kV and at a nominal magnification of 75,000 ×. Images (0.91 Å/pixel) were recorded at applied underfocus values ranging from approximately -1.0 to -3.0 µm on a Falcon II direct electron detector (FEI) as 16 frames in 1.0 s exposure with a total electron dose of 20 electrons/Å$^2$. Data were subsequently aligned and summed using MotionCor2[10] to obtain a final dose weighted image and then 2× binning was performed using the Bsoft program package,[11] resulting in a pixel size of 1.82 Å for further image processing. Estimation of the contrast transfer function was performed using

CTFFIND4.[12] Micrographs exhibiting poor power spectra based on the extent and regularity of the Thon rings were rejected. Initially, approximately 2,000 particles were manually picked from 43 micrographs and subjected to reference-free two-dimensional (2D) classification using EMAN 2.1.[7] Ten representative 2D class averages were selected as templates for automated particle picking using Gautomatch (http://www.mrc-lmb.cam.ac.uk/kzhang/). All subsequent processing steps were performed in RELION 2.0.[9] A total of 131,812 auto-picked particles from 2,637 micrographs were subjected to reference-free 2D classification to remove aberrant particles. Particles in 22 representative classes showing spherical shapes were selected (58,157 particles) for the following processes. The selected particles were subjected to three-dimensional (3D) structure refinement and post-processing without any symmetry (C1 symmetry), where the initial low-resolution structure as described above was used for the reference in the 3D classification after low-pass filtered to 60 Å. The resolution was estimated to 5.6 Å by the gold-standard Fourier shell correlation (SCF = 0.143 criterion), after applying a soft spherical mask on the two reconstructions refined from the half of the data sets independently. The resultant map clearly showed the overall TRAP-cage structure having 24 11-membered rings with D4 symmetry. However, the individual ring structure showed mixed features of two mirrored protein structures described below. Further structure analysis was carried out using TRAP-cage formed using Au-TPPMS rather than GNPs.

*Cryo-EM single particle reconstruction of TRAP-cage formed using Au-TPPMS at higher resolution*

A purified sample (3 µl of 0.89 mg/ml) formed using Au-TPPMS was applied to glow-discharged holey carbon grids (Quantifoil R 1.2/1.3, Mo 200 mesh) with a thin amorphous carbon film of ~10 nm thickness over the holes and incubated for 30 s at 4 °C and 100% humidity. Grids were then blotted for 3.0 s and plunged into liquid ethane using a Vitrobot Mark IV (FEI). Data were recorded semi-automatically using the EPU software on a transmission electron cryo-microscope (FEI Titan Krios) operated at an accelerating voltage of 300 kV and at a nominal magnification of 75,000 ×. Images (0.91 Å/pixel) were recorded at

applied underfocus values ranging from approximately -0.9 to -3.4 μm on a Falcon II direct electron detector (FEI) as 32 frames in 2.0 s exposure with a total electron dose of 40 electrons/Å$^2$. Data were subsequently aligned and summed using MotionCor2[10] to obtain a final dose weighted image and then 2× binning was performed using the Bsoft program package,[11] resulting in a pixel size of 1.82 Å for further image processing. Estimation of the contrast transfer function was performed using CTFFIND4.[12] Micrographs exhibiting poor power spectra based on the extent and regularity of the Thon rings were rejected (96 micrographs). Initially, approximately 2,000 particles were manually picked and subjected to reference-free two-dimensional (2D) classification using EMAN 2.1.[7] Ten representative 2D class averages were selected as templates for automated particle picking using Gautomatch (http://www.mrc-lmb.cam.ac.uk/kzhang/). All subsequent processing steps were performed in RELION 2.0.[9] A total of 1,085,623 auto-picked particles from 10,290 micrographs were subjected to reference-free 2D classification to remove aberrant particles. Particles in 5 representative classes showing spherical shapes were selected (578,865 particles) for the following processes. The selected particles were subjected to three-dimensional (3D) classification into three classes using an angular sampling of 3.7° for 25 iterations without any symmetry (C1 symmetry), where the initial low-resolution structure as described above was used for the reference in the 3D classification after low-pass filtered to 60 Å. The particles (176,463 particles) in a class showing the most symmetrical cage structure with regular density distribution were selected for the following processes. However, although the density map clearly showed the overall TRAP-cage structure as a sphere with 24 11-membered rings, the structure at the level of the individual rings was curiously devoid of protein chiral features and showed mixed features of two mirrored protein structures, contrary to expectations from the protein structure previously determined by x-ray crystallography,[1] which is suggestive of the existence of chiral cage structures. Therefore, to separate the two chiral cage particles, we performed a second round of 3D classification into two classes using a finer angular sampling of 1.8° for 25 iterations without any symmetry (C1 symmetry). The resultant two maps clearly showed left-handed and right-handed structures at the level of the individual protein rings, respectively. Each structure (class I: 94,338 particles

and class II: 82,125 particles) was refined individually with the C1 (asymmetric reconstruction), C4 and D4 symmetries. The resolutions of the class I were estimated as 3.7 (octahedral symmetry), 3.9 (D4), 4.1 (C4), and 4.4 Å (C1) and the resolutions of the class II were estimated to 3.9 (D4 sym.), 4.2 (C4 sym.), and 4.5 Å (C1 sym.) by the gold-standard Fourier shell correlation (FSC = 0.143 criterion), after applying a soft spherical mask on the two reconstructions refined from the half of the data sets independently. According to the individual protein structures, the handedness of the class I map was corrected to the opposite one (resulting in class I: right-handed cage structures and class II: left-handed cage structures). The maps of the class I and II with octahedral symmetry were sharpened with B-factors of -236 and -244 $Å^2$, respectively. Local resolution was estimated using ResMap.[13] Figures were prepared using UCSF Chimera.[14]

*Structural refinement*

The initial atomic coordinate model was based on the TRAP crystal structure (PDB accession 4V4F[9]), with the $Cys^{35}$ and $Ser^{64}$ substitutions modelled in Coot[15] to generate $TRAP^{CS}$ ring structures. Note that residue positions have been renumbered from the initial deposited PDB to reflect the actual positions in the coding sequence of TRAP from *G. stearothermophilus* (e.g. the mutated Lys->Cys residue was assigned to residue number 37 in the original PDB file 4V4F but corresponds to residue number 35 in our analyses). Initial inspection of the density maps revealed areas of weak or missing density, and thus the structure of each TRAP subunit was truncated to residues 6-72; in addition residues 22-32 (corresponding to a loop that exhibits high flexibility in the *apo*-form of TRAP[16]) were omitted from the model to reflect this. Refinement of the LH and RH structures followed a similar regime. Twenty-four copies of $TRAP^{CS}$ rings were initially fit into the cage density by rigid body refinement using Phenix real-space refinement.[17] Optimization of the original cryo-EM map voxel size using the high-resolution TRAP crystal structure[1] as a reference was performed as follows, in a manner analogous to previous reports.[18,19] Comparison of cross-correlation scores of the fits between a simulated map of the $TRAP^{CS}$ ring atomic model and the cryo-EM map at varying voxel scales

(starting from the original 1.82 Å voxel$^{-1}$ and varying by 0.01 increments) was performed using Chimera, with the optimal results corresponding to a map scale of 1.74 Å voxel$^{-1}$. Similar results were obtained by performing rigid body refinement of individual subunits of 24 TRAP$^{CS}$ rings onto the cryo-EM density at varying scales using Phenix.[17] Au$^{I}$ atoms (120 in total) were docked manually into the prominent blobs of density between the Cys$^{35}$ side chains from neighbouring rings of the rigid-body fitted model, and subsequently 15 macro cycles of Phenix real-space refinement were run using the 1.74 Å voxel$^{-1}$ map, including rigid-body refinement, global minimization, a single round of simulated annealing, and adp refinement; restraints on the Au-S bond lengths and S-Au-S bond angles were applied during the later stages of refinement. Validation of the refined models was carried out using MolProbity.[20] Analysis of interfacial contacts in the TRAP-cage models was performed using PDBePISA (http://www.ebi.ac.uk/pdbe/pisa/).[21]

*Transmission electron microscopy (TEM)*

Samples were typically diluted to a final protein concentration of 0.025 mg/ml, centrifuged briefly in a desktop centrifuge and the supernatant applied onto hydrophilized carbon-coated copper grids (STEM Co.), negatively stained with 3 % phosphotungstic acid, pH 8, and visualized using a JEOL JEM-1230 80 kV instrument.

*Native PAGE*

Samples were run on 3-12% native Bis-Tris gels following the manufacturer's recommendations (Life Technologies). Samples were mixed with 4x native PAGE sample buffer (200 mM BisTris, pH 7.2, 40% w/v Glycerol, 0.015% w/v Bromophenol Blue). As a qualitative guide to molecular weights of migrated bands, NativeMark unstained protein standard (Life Technologies) was used. Where blue native PAGE was performed, protein bands were visualized according to the manufacturer's protocol (Life Technologies), otherwise InstantBlue$^{TM}$ protein stain (Expedeon) was used.

*Electrothermal atomic absorption spectrometry (ETAAS)*

A sample mass of 2 mg was dissolved in 25 ml with 0.2 % HCl. The solution was then diluted 25 × before determination of total Au performed by an ETAAS spectrometer (PinAAcle 900Z, Perkin Elmer, Waltham, MA), with Zeeman background correction, at a wavelength of 242.80 nm (slit width of 0.7 nm). The measured volume of the sample solution was 10 µl and to each sample a mixture of matrix modifiers: 5 µg of $Pd(NO_3)_2$ and 3 µg of $Mg(NO_3)_2$ was added. Five sets of measurements were carried out with each set consisting of three repeats.

*Proton-induced X-ray emission (PIXE)*

The TRAP-cage structural model has a bridging gold atom between 10 of the 11 $Cys^{35}$ residues of each TRAP ring. Given the presence of an additional sulphur atom per TRAP monomer (from methionine) this would give a ratio of S:Au of 4.4:1 assuming that the $Cys^{35}$ at the $11^{th}$ monomer of each ring did not bind a gold or 3.7:1 assuming that it did. The S:Au ratio was determined using Micro-PIXE measurements performed with a high energy focused proton beam (nuclear microprobe) in the tandem accelerator laboratory of the Jožef Stefan Institute.[22] The beam is focused by a magnetic quadrupole triplet lens and scanned over the square-shaped area of interest by magnetic deflectors. The micro-PIXE setup is described in detail by Vavpetič et al.[23] X-ray analysis was carried out by a Peltier-cooled silicon drift detector (SDD), equipped with ultra-thin vacuum window and aluminum-coated 1 micrometer thick mylar foil to block visible light photons.

Standard sample substrate for micro-PIXE analysis was used for the protein analysis, consisting of a 100 nm thick pioloform foil spanned over 0.5 mm thick aluminium frame with 8 mm aperture. TRAP (approx. 0.5 mg/ml) was applied to the centre of the aperture as two consecutive depositions of 0.5 µl and dried. The second deposition took place after complete drying of the first. Sample was mounted on the sample holder and inserted into the high vacuum system with a vacuum of $2 \times 10^{-7}$ mbar. We applied a 3 MeV beam with a diameter of 1.0 micrometre and beam current of 200 pA. The transmitted proton beam was detected with a dedicated beam stopper incorporating on-off axis detector for Scanning Transmission Ion

Microscopy (on-off axis STIM[24]) providing the sample thickness information. The beam was scanned across the selected field of interest, varying from maximum scanning field of 2000 × 2000 μm$^2$ down to 400 × 400 μm$^2$. All the measurements were taken in the listmode, which enables data sequence recovery and monitoring of eventual sample evolution during the measurements. The methodology of the micro-PIXE protein analysis was adopted according to published methods.[25] For the quantification, the samples were treated as samples of finite thickness, and proton beam stopping as well as X-ray attenuation in the sample were taken into account within the Gupixwin program.[26] The precision of the method was validated during each set of experiments by measurement of reference pure metals of Al, Ti, Cu and Au, Standard Reference Material of the National Institute for Standards and Technology (NIST) Naval Brass (C1107) and a set of thin evaporated XRF reference samples of Au and $CuS_x$ produced by the Micromatter company (Canada).

*X-ray photoelectron spectroscopy (XPS)*

XPS analysis was performed on a VersaProbeII PHI scanning XPS spectrometer with Al Kα monochromatic X-ray (1486.6 eV) excitation with a beam diameter of 100 μm on a 400 μm x 400 μm surface. The angle of the photoelectron analysis was 45° and the energy of electrons in the analyzer was equal to 46.95 eV. A dual neutralizer was applied on the test surface with the help of an Ar+ ion beam with energy 7 eV and electrons with energy 1 eV. The XPS binding energies were calibrated using the carbon 284.80 eV 1s peak. The Pressure inside the chamber was $4x10^{-9}$ mbar. Deconvolution and spectra analysis was done in the PHI MultiPak program (version 9.8.0.19).

*Liquid-chromatography mass spectrometry*

Purified TRAP-cage was denatured in 50 mM Tris·HCl buffer (pH 8.0) with 8 M urea at 56 °C for 30 min, then buffer-exchanged to 50 mM Tris·HCl buffer (pH 8.0) using a centrifugal filtration device (Amicon 3 kDa MWCO, Millipore). For denaturing LC-MS analysis, the TRAP protein was desalted on a C18 pre-column (Acclaim PepMap100, C18, 300 μm × 1 cm;

Thermo Scientific), then separated on a C18 column (Acclaim PepMap100, C18, 75 µm × 15 cm; Thermo Scientific) by a Dionex UltiMate 3000 RSLCnano System connected to a hybrid LTQ Orbitrap XL mass spectrometer (Thermo Scientific) via a dynamic nanospray source. A binary buffer system was used, with buffer A 0.1% formic acid in $H_2O$, and buffer B 0.1% formic acid in acetonitrile. The proteins were separated at 25 °C with a gradient of 1 % to 90 % buffer B at a flow rate of 300 nL $min^{-1}$ over 60 min. The LTQ-Orbitrap XL was operated in positive ion mode with a nanoelectrospray voltage of 1.6 kV and capillary temperature of 275 °C. Survey full-scan MS spectra were acquired in the orbitrap (*m/z* 300−4000) with a resolution of 60000. The data were processed using Xcalibur 2.2 (Thermo Scientific).

*Native mass spectrometry*

TRAP-cage samples at 0.8 mg/ml were prepared for native MS by buffer-exchanging into ammonium acetate (pH 6.9) using miniature spin columns (Micro Bio-Spin P-6, BioRad). This was performed in two steps: the first exchanged into 2.5 M ammonium acetate, the second into 200 mM ammonium acetate. Native MS experiments were performed using methods described previously,[27] employing a Q-ToF2 instruments (Waters Corp.), modified for the analysis of large protein ions.[28] Relevant instrument parameters were: nanoelectrospray capillary voltage: 1.9 kV; sample cone: 200 V; extractor cone: 10 V, acceleration into collision cell: 200 V. The collision cell was pressurized with argon at ≈35 µbar. Data was calibrated externally using MassLynx software (Waters Corp.) and are shown without background subtraction and minimal smoothing.

*Raman spectroscopy*

Raman spectra were collected for TRAP-cage proteins in powder form and oxidized and reduced glutathione (Sigma) and for oxidised and reduced $TRAP^{CS}$ rings. Spectra were collected using a Renishaw InVia Raman spectrometer equipped with a confocal microscope and CCD camera (1024 × 256 pixels). The excitation wavelength was provided by a diode laser emitting at 532.0 nm. All spectra were acquired with a spectral resolution of 4 $cm^{-1}$ in the

spectral range of 100–3200 $cm^{-1}$ using 20 × objective. The exposure time was 30 s with four acquisitions averaged to a single spectrum. The spectra were smoothed using 13 points Savitzky-Golay filter, baselined using a rubber band algorithm and normalized to maximal intensity.

*Mathematical modelling of TRAP-cage*

We modelled the TRAP ring as a unit circle with 11 evenly spaced vertices on its perimeter. Assuming that the TRAP-cage has octahedral symmetry, then the complete cage can be assembled from this canonical ring by transformations about the 24 rotations in the octahedral group. The paradoxical cage in Fig. 4b suggests a set of 120 pairs of simulated S-Au-S bonds, one for each location where two hendecagonal vertices meet. For any given position and orientation of the canonical ring, the 24 rotated images in the simulated TRAP-cage will yield a set of 120 bond lengths. Our goal was to derive the six numbers defining the position and orientation of the canonical ring so that these 120 bonds are as close as possible in length to the ideal value of 4.7 Å. We can find a near-optimal position and orientation using numerical optimization, resulting in a configuration of TRAP rings, where the ideal value is matched to within an error of $5\times10^{-9}$ Å, i.e. essentially to within numerical accuracy and which is well within the physical tolerances for actual S-Au-S coordination bonds.

The optimal arrangement of TRAP rings was computed using a custom-written C++ program of about 1000 lines of code. The core of the program uses the code for the "downhill simplex" method of continuous simulated annealing, as provided in Press et al.[29] The program also uses the Boost library (www.boost.org) for quaternions and random number generation. 3D visualizations were modelled and rendered in Rhinoceros 3D by Robert McNeel and Associates (www.rhino3d.com); the output from the optimizer was used to transform TRAP rings into position using a custom Python script

*Prediction of other paradoxical cages*

To predict the geometry of other nearly regular cages, assemblies made of identical regular *n*-gons, for n = 7, 8, … 17 were considered. These polygonal faces were placed on the vertices of regular polyhedra so that the faces of the polyhedron correspond to the holes of the cage and the edges of the polyhedron, to the links between adjacent faces of the cage. The polyhedra used for this "dressing" method included all Platonic and Archimedean solids, prisms and anti-prisms, ignoring those with faces having more than 6 edges. We wrote a computer program to construct many of the possible convex geometries from the method described above. The C++ program (of around 3000 lines of code) outputs a file describing the topology, i.e. the links between all the faces, for each potential cage thus found.

A second C++ program (about 8400 lines of code) was then used to derive the geometric properties of the prospective cages. First the polygonal faces were modelled as rigid bodies, with adjacent faces linked by two Hookean springs with a rest position set to 5% of the edge length. The energy of the system was then minimised using a Monte Carlo algorithm. The coordinates of the resulting polyhedron were then used by the program to model the cage as a set of rigid rods using an energy functional consisting of three terms: edge length deviations, face edge angular deviations, and degree of non-planarity. The first one measured by how much the edge lengths deviated for a chosen reference length. The second one measured by how much the angle between the face edges deviated from the angle of the regular polygon. The third term was measuring the level of non-planarity of the faces. Each term was multiplied by a weight factor, with the planarity weight set to three orders of magnitude larger than for the lengths and the angles. This allowed us to obtain structures with planar faces (with zero planarity distortions modulo numerical error). The energy functional was minimised using a Monte Carlo method, with the program generating a file containing the coordinates of each vertex, the topology of the cage, as well as the range of deformations obtained for the angles and edge lengths. A detailed description of the algorithm will be given in a future publication.

Of the thousands of cages generated by the method described above, we selected candidates for which the level of deformation for both angles and edge lengths was smaller than 1%. In some cases, e.g. the cage shown in Fig. 4d, the basic structure was obtained by manual

construction of a physical model, with the topology then being fed into the second program for optimisation.

**Code Availability**

Custom codes used to compute the optimal arrangement of TRAP rings and to predict paradoxical cages are available from the authors on reasonable request

**Data Availability**

The data that support the findings of this study are available via the corresponding author on reasonable request. The cryo-EM density maps have been deposited in the Electron Microscopy Data Bank under accession codes EMD-6966 (GNP-produced TRAP-cage), EMD-4443 (Left-handed TRAP-cage) and EMD-4444 (right-handed TRAP-cage) the coordinates have been deposited in the Protein Data Bank under accession numbers 6IB3 (left-handed TRAP-cage) and 6IB4 (right-handed TRAP-cage).

**Methods References**


1 Hopcroft, N. H. *et al.* The interaction of RNA with TRAP: the role of triplet repeats and separating spacer nucleotides. *J. Mol. Biol.* **338**, 43-53, (2004).

2 Yang, F., Moss, L. G. & Phillips, G. N., Jr. The molecular structure of green fluorescent protein. *Nat. Biotechnol.* **14**, 1246-1251, (1996).

3 Young, G. *et al.* Quantitative mass imaging of single biological macromolecules. *Science* **360**, 423-427, (2018).

4 Cole, D., Young, G., Weigel, A., Sebesta, A. & Kukura, P. Label-Free Single-Molecule Imaging with Numerical-Aperture-Shaped Interferometric Scattering Microscopy. *ACS Photonics* **4**, 211-216, (2017).

5 Li, X. *et al.* Electron counting and beam-induced motion correction enable near-atomic-resolution single-particle cryo-EM. *Nat. Methods* **10**, 584-590, (2013).

6 Yasunaga, T. & Wakabayashi, T. Extensible and object-oriented system Eos supplies a new environment for image analysis of electron micrographs of macromolecules. *J. Struct. Biol.* **116**, 155-160, (1996).

7 Tang, G. *et al.* EMAN2: an extensible image processing suite for electron microscopy. *J. Struct. Biol.* **157**, 38-46, (2007).

8 Ludtke, S. J., Baldwin, P. R. & Chiu, W. EMAN: semiautomated software for high-resolution single-particle reconstructions. *J. Struct. Biol.* **128**, 82-97, (1999).

9 Scheres, S. H. RELION: implementation of a Bayesian approach to cryo-EM structure determination. *J. Struct. Biol.* **180**, (2012).

10 Zheng, S. Q. *et al.* MotionCor2: anisotropic correction of beam-induced motion for improved cryo-electron microscopy. *Nat. Methods* **14**, 331-332, (2017).

11 Heymann, J. B. Bsoft: image and molecular processing in electron microscopy. *J. Struct. Biol.* **133**, 156-169, (2001).

12 Rohou, A. & Grigorieff, N. CTFFIND4: Fast and accurate defocus estimation from electron micrographs. *J. Struct. Biol.* **192**, 216-221, (2015).

13 Kucukelbir, A., Sigworth, F. J. & Tagare, H. D. Quantifying the local resolution of cryo-EM density maps. *Nat. Methods* **11**, 63-65, (2014).

14 Pettersen, E. F. *et al.* UCSF Chimera--a visualization system for exploratory research and analysis. *J. Comput. Chem.* **25**, 1605-1612, (2004).

15 Emsley, P., Lohkamp, B., Scott, W. G. & Cowtan, K. Features and development of Coot. *Acta. Cryst. D* **66**, 486-501, (2010).

16 Malay, A. D., Watanabe, M., Heddle, J. G. & Tame, J. R. H. Crystal structure of unliganded TRAP: implications for dynamic allostery. *Biochem. J.* **434**, 429-434, (2011).

17 Adams, P. D. *et al.* PHENIX: a comprehensive Python-based system for macromolecular structure solution. *Acta. Cryst. D* **66**, 213-221, (2010).

18 Wang, Z. *et al.* An atomic model of brome mosaic virus using direct electron detection and real-space optimization. *Nat. Commun.* **5**, 4808, (2014).

19 Natchiar, S. K., Myasnikov, A. G., Kratzat, H., Hazemann, I. & Klaholz, B. P. Visualization of chemical modifications in the human 80S ribosome structure. *Nature* **551**, 472-477, (2017).

20 Chen, V. B. *et al.* MolProbity: all-atom structure validation for macromolecular crystallography. *Acta. Cryst. D* **66**, 12-21, (2010).

21 Krissinel, E. & Henrick, K. Inference of macromolecular assemblies from crystalline state. *J. Mol. Biol.* **372**, 774-797, (2007).

22 Pelicon, P. *et al.* A high brightness proton injector for the Tandetron accelerator at Jožef Stefan Institute. *Nucl. Instrum. Meth. B* **332**, 229-233, (2014).

23 Vavpetič, P., Kelemen, M., Jenčič, B. & Pelicon, P. Nuclear microprobe performance in high-current proton beam mode for micro-PIXE. *Nucl. Instrum. Meth. B* **404**, 69-73, (2017).

24 Pallon, J. *et al.* An off-axis STIM procedure for precise mass determination and imaging. *Nucl. Instrum. Meth. B* **219**, 988-993, (2004).

25 Garman, E. F. & Grime, G. W. Elemental analysis of proteins by microPIXE. *Prog. Biophys. Mol. Bio.* **89**, 173-205, (2005).

26 Campbell, J. L., Hopman, T. L., Maxwell, J. A. & Nejedly, Z. The Guelph PIXE software package III: alternative proton database. *Nucl. Instrum. Meth. B* **170**, 193-204, (2000).

27 Kondrat, F. D., Struwe, W. B. & Benesch, J. L. Native mass spectrometry: towards high-throughput structural proteomics. *Methods Mol. Biol.* **1261**, 349-371, (2015).

28 Sobott, F., Hernandez, H., McCammon, M. G., Tito, M. A. & Robinson, C. V. A tandem mass spectrometer for improved transmission and analysis of large macromolecular assemblies. *Anal. Chem.* **74**, 1402-1407 (2002).

29 Press, W. H., Teukolsky, S. A., Vetterling, W. T. & Flannery, B. P. *Numerical recipes in C (2nd ed.): the art of scientific computing*. (Cambridge University Press, 1992).

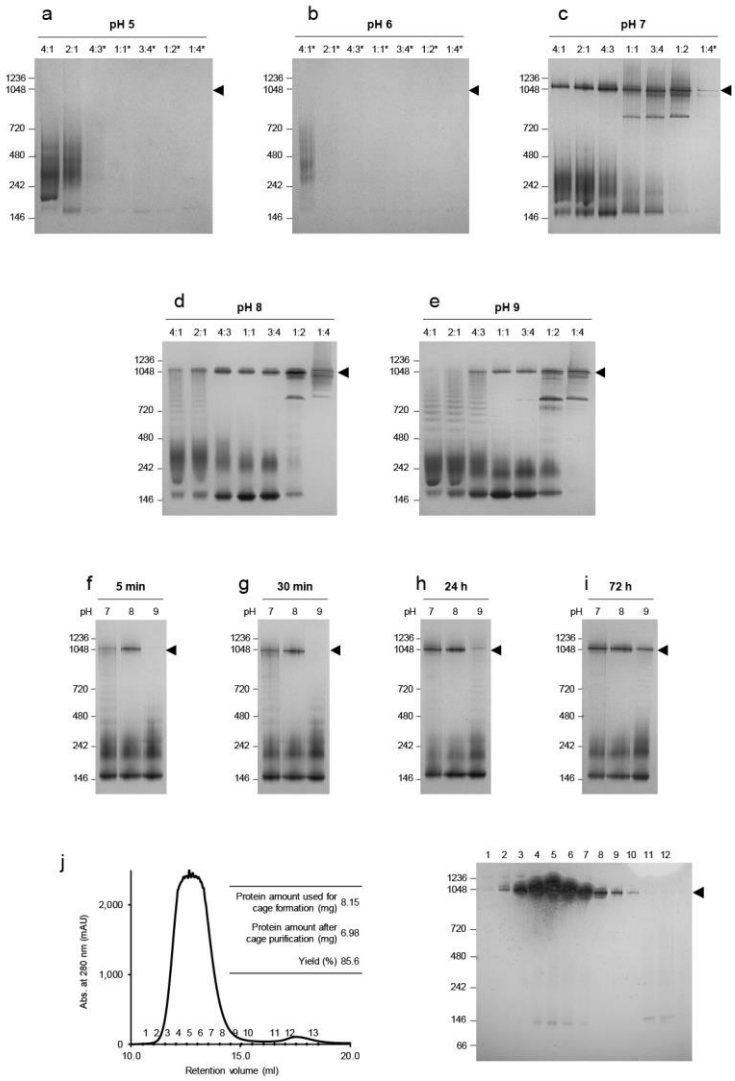


**Extended Data Figure 1. Optimization of conditions for TRAP-cage formation. a-e,** Effect of pH on cage formation. Reactions containing 0.8 mg/ml TRAP$^{CS}$ were incubated with Au-TPPMS at the indicated pH values for 3 days, spun down on a desktop centrifuge and subjected to blue native PAGE. The ratios denote TRAP$^{CS}$ monomer : Au(I) molar ratios. Formation of white precipitate was detected in the reactions marked with an asterisk, and correlates with a decrease in band intensity. **f-i,** Time course of TRAP-cage formation at pH 7, 8, and 9, visualized by blue native PAGE. Each reaction contains Au-TPPMS and 0.8 mg/ml TRAP$^{CS}$ at a 1:1 molar ratio. Total incubation times are indicated above each gel. Gels **a-i** were repeated once, giving similar results. **j**, Left, product of reaction containing 8.15 mg TRAP$^{CS}$ and Au-TPPMS under standard cage-formation conditions was subjected to SEC using a Superose 6 Increase 10/300 GL column and fractions collected as indicated. Right, native PAGE of

fractions 1-13 demonstrates they contain almost exclusively cage structures. Inset table demonstrates high recovery yields of TRAP-cage based on $A_{280}$ measurements of initial and purified samples. SEC is representative of two independent experiments, giving similar results. Positions of molecular weight marker bands are indicated to the left of gels and arrowheads indicate the position of bands corresponding to TRAP-cage. For gel source data, see Supplementary Figure 1.

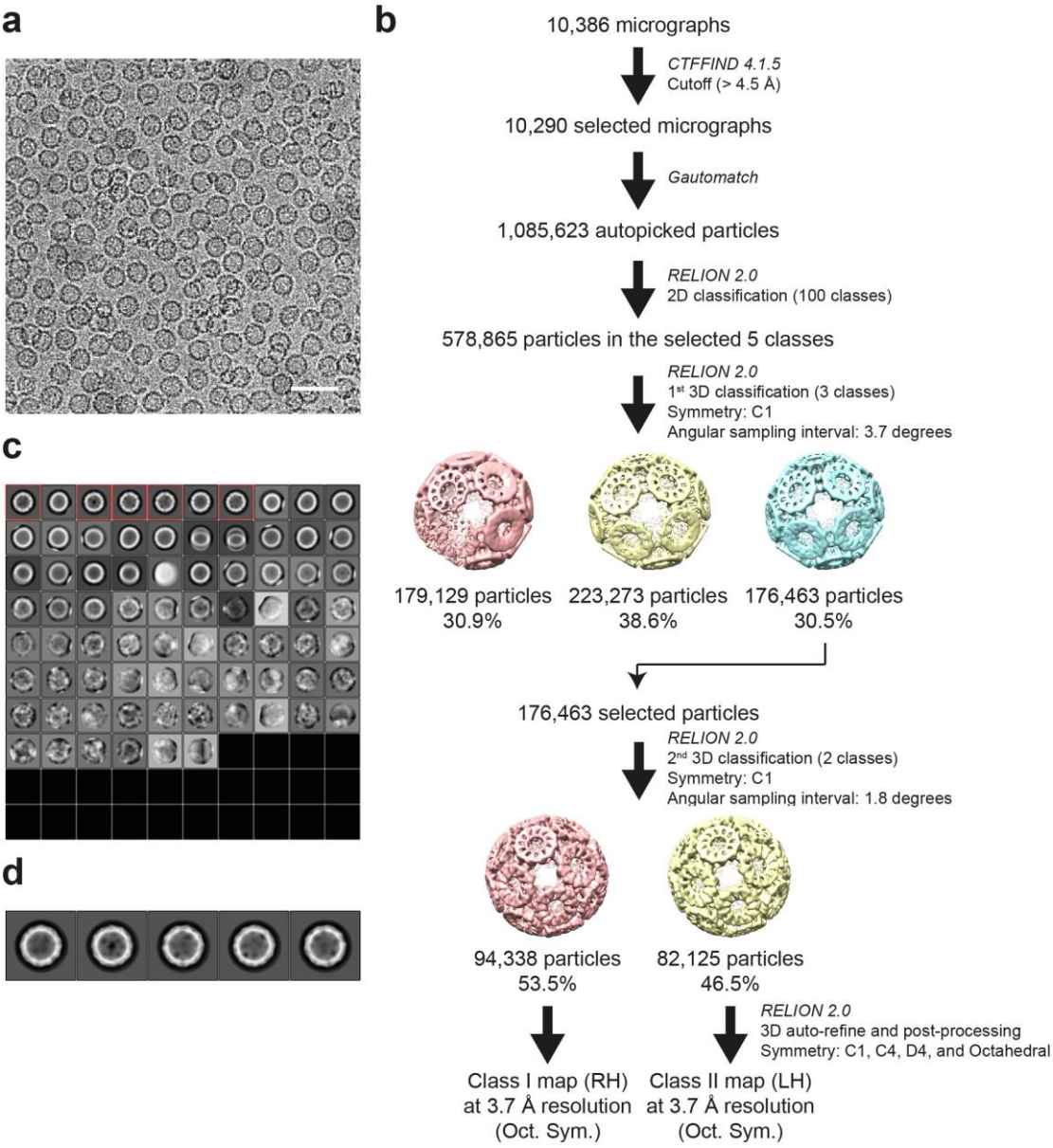


**Extended Data Figure 2. Procedure for cryo-EM single-particle reconstruction for TRAP-cage formed with Au-TPPMS. a,** Representative micrograph of the TRAP-cage.

Scale bar = 50 nm. **b,** Summary of the image processing procedure (see Methods). **c,** 2D class averages from reference-free 2D classification by RELION 2.0. The selected 2D class averaged images (5 classes including 578,865 particles) for further image processing are highlighted with red squares. **d,** The selected five 2D classes (box size: 220 × 220 pixels, 382.8 × 382.8 Å).

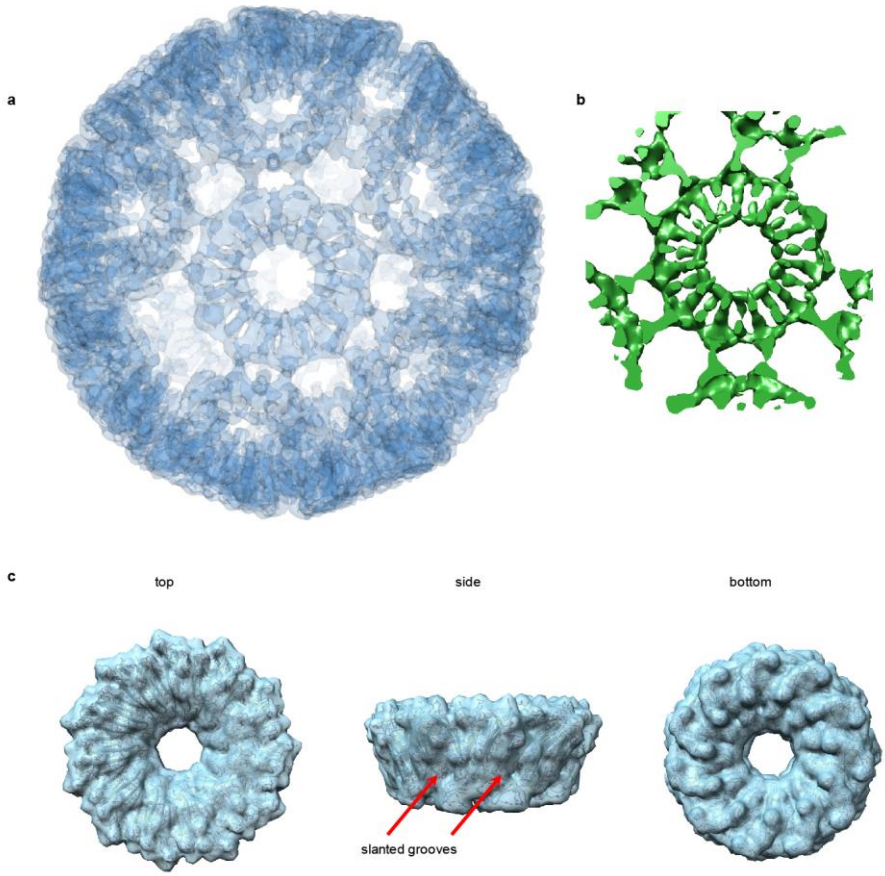


**Extended Data Figure 3. Initial density map of TRAP-cage displaying aberrant features.** **a-b**, the initial cryo-EM map, refined to 5.6 Å resolution, showing a distinct lack of chirality at the level of the individual rings. **a**, Overall map depicted in transparency, shows ring densities resembling radial wheel spokes. **b**, Close-up on a ring density at low contour level, viewed from the interior of the cage, showing exclusively radial features (densities and gaps). **c**, For comparison, the atomic model of $TRAP^{CS}$ (based on PDB ID 4V4F), is simulated to a resolution of 5.9 Å, showing that chiral properties (*e.g.* curved propeller-like features, slanted grooves) should be readily visible on the rings at this resolution.

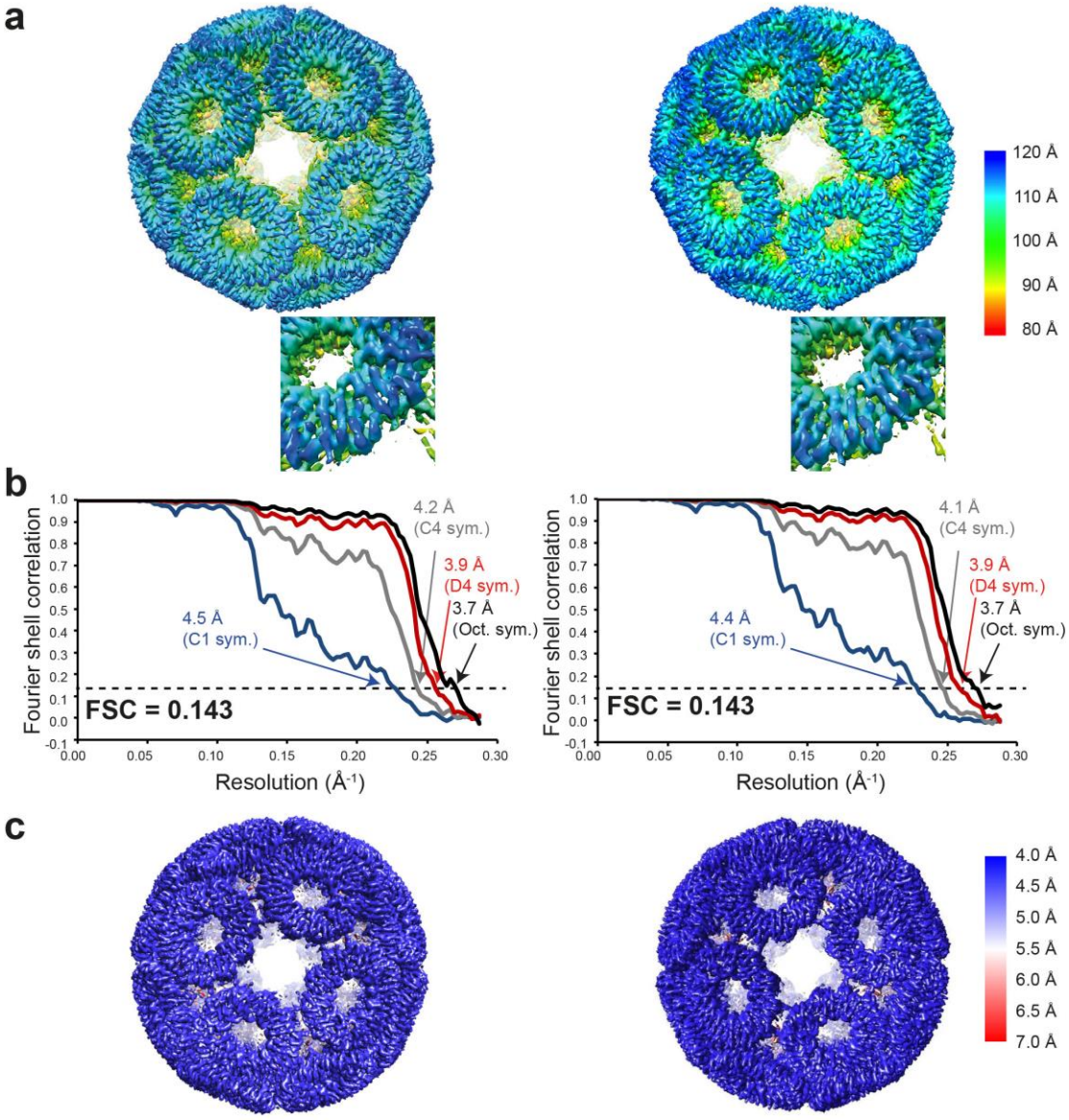


**Extended Data Figure 4. Map quality and resolution for TRAP-cage formed with Au-TPPMS.** LH and RH cages are shown on the left and right, respectively. **a,** Surface representations coloured according to the distance from the centre of the particle. **b,** Gold-standard FSC curve for the cryo-EM map of LH and RH cages with C1, C4, D4, and Octahedral (Oct) symmetries from 94,338 and 82,125 particles, respectively. The estimated resolutions at 0.143 criterion for the maps with octahedral symmetry were 3.7 Å. **c**, The refined density maps coloured by local resolution in surface view.

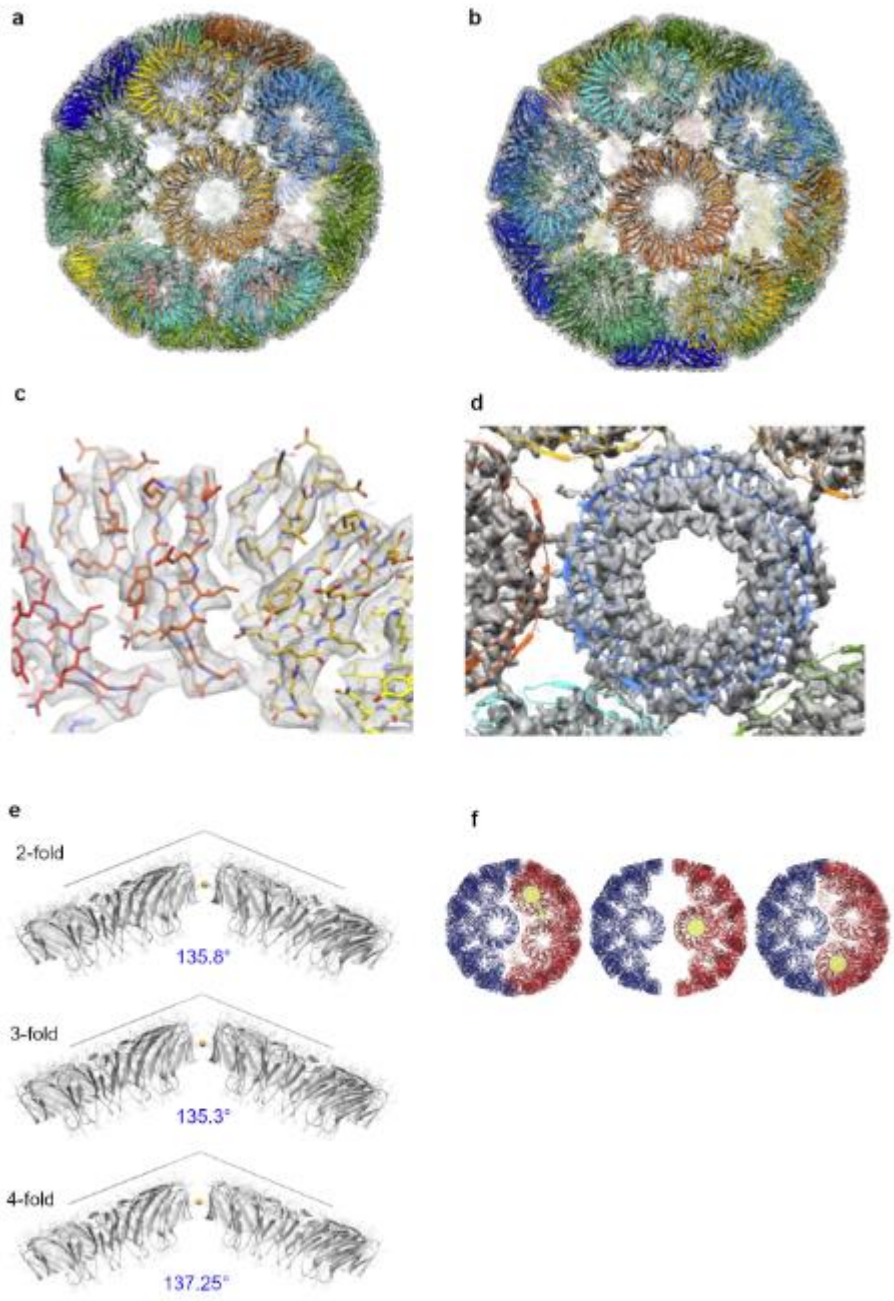


**Extended Data Figure 5. Details of the refined TRAP-cage structure. a-b**, Overall fits of the final TRAP-cage models onto their respective density maps: (**a**) LH and (**b**) RH structures. Cysteine residues are rendered as ball and stick while gold atoms are shown as spheres. **c**, Close-up of the LH cage, to show fitting of $TRAP^{CS}$ structural elements into the density. **d**, Close-up of the interior of the LH cage, showing flexible loop (residues 23-32) with missing density, consistent with non-tryptophan-bound TRAP structure[1]. **e**, Slightly unequal dihedral angles are formed between neighbouring $TRAP^{CS}$ rings in the final TRAP-cage model,

averaging 135.8°, 135.3°, and 137.25° around the 2-, 3-, and 4-fold rotational axes, respectively, with a mean value of 136.2° across the entire cage. It is notable that in the canonical pentagonal icositetrahedron, a constant dihedral angle of 136.3° is formed between any two adjacent faces. **f**, The equivalence of the two chiral forms of TRAP-cage may explain their roughly equal proportions and is clear if the cage assemblies are decomposed into two congruent hemispheres of 12 rings each. The hemispheres are themselves *achiral*, but together two can take either chiral form depending on their relative orientations when assembled. The two chiral forms can be interconverted through the relative rotation of hemispheres by about 24.1°. In the figure, each achiral half of the cage coloured in red and blue, and the relative rotation can be tracked as the change in position of the highlighted ring in the direction of the arrow.

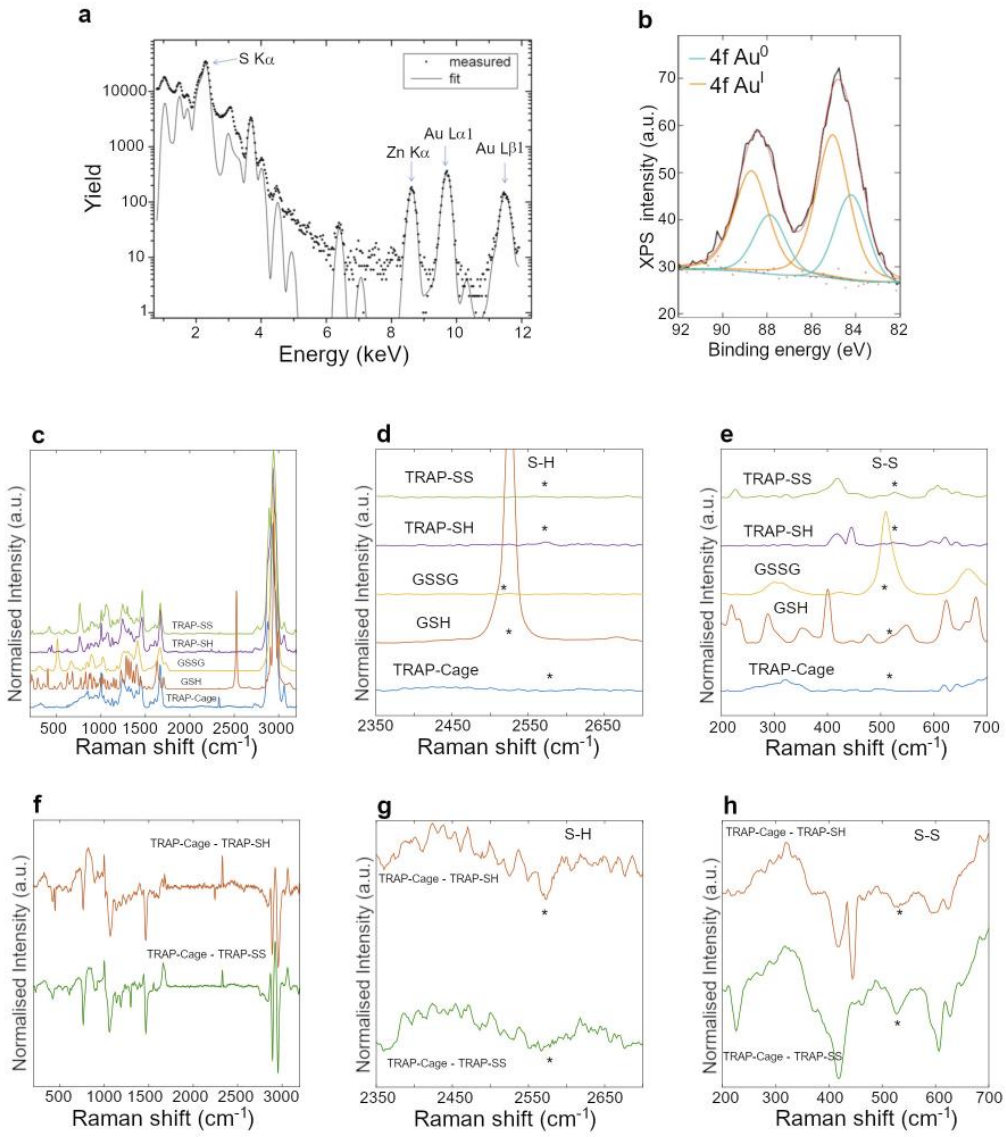


**Extended Data Figure 6. Confirmation and quantitation of Au in the TRAP-cage. a**, Micro-PIXE measurements of purified TRAP-cage showing X-ray spectrum. Au L peaks and the S K peak were used to estimate the S:Au molar ratio in the sample, which was calculated to a range of approximately 5.1 - 6.9 Au per sulphur. The dots represent the measured data, while the continuous line represents the fit with the Gupixwin program.[2] Results are representative of two independent experiments, each giving similar results. **b**, Au 4*f* XPS spectra (black line) of the TRAP-cage with the expected spectra for $Au^0$ and $Au^I$ shown in blue and orange, respectively. The cumulative fit (red) and residuals (red squares) are also shown. The shift in binding energy from 84.19 to 84.99 of (i.e. 0.85 80) eV matches well with Au-S reported previously[3,4]. The presence of signal in the $Au^0$ binding energy range can be attributed

to a weakly interacting Au coordination bond with the second S in the bridge, since repeated measurements of different purification methods excluded the chance of X-ray degradation or unreacted substrates giving $Au^0$ signal. **c**-**h**, Raman spectroscopy suggests the absence/low abundance of S-S and S-H bonds in TRAP-cage. **c**, Raman spectra of TRAP-cage, oxidised and reduced TRAP-rings (TRAP-SS and TRAP-SH respectively), with oxidized and reduced glutathione (GSSG and GSH, respectively), showing the full spectral range. **d** and **e** show enlargements of the S-H vibration and S-S vibration regions, respectively. Locations of peaks corresponding to S-S and S-H vibrations are labelled with asterisks. Since the exact positions depend on the molecular species and its conformation, the peak maxima for glutathione are shifted relative to cysteine-based signals (e.g. 509-540 $cm^{-1}$ range for S-S vibrations).[5] As some peaks corresponding to S-H and S-S bonds were small, their absence from the TRAP-cage spectra were assessed by subtracting relevant spectra (i.e. TRAP-SS or TRAP-SH) for TRAP-rings from the TRAP-cage data. **f**, the resulting spectra shown in the full spectral range. **g** and **h**, enlargements of the relevant regions. Spectra after normalization were offset for clarity. For XPS and Raman spectra, experiments were independently repeated at least once, each giving similar results.

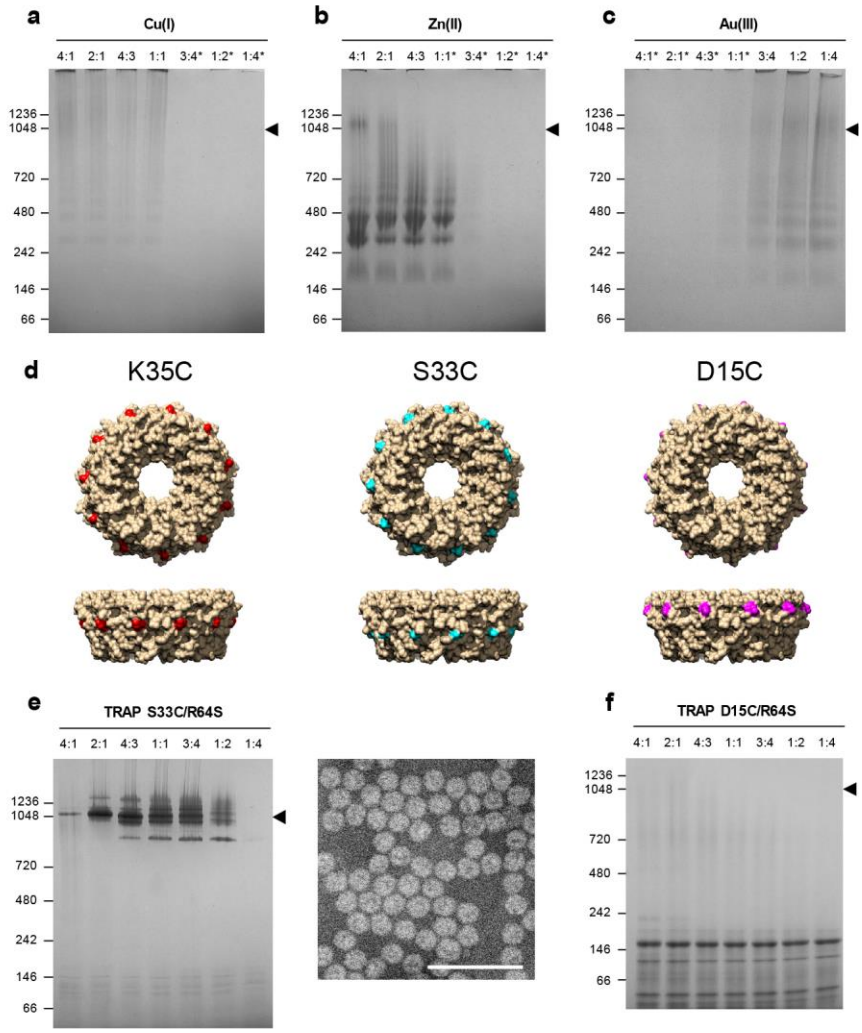


**Extended Data Figure 7. Further probing TRAP-cage assembly. a-c,** Testing the ability of different metal ions to trigger protein cage formation. Reactions containing 0.8 mg/ml $TRAP^{CS}$ were incubated under standard cage-formation conditions except Au-TPPMS was replaced with the indicated metal ions, then spun down on a desktop centrifuge and subjected to blue native PAGE. $TRAP^{CS}$ monomer : metal ion molar ratios are indicated above each lane. $TRAP^{CS}$ was incubated with (**a**) $Cu^{I}$, (**b**) $Zn^{II}$, and (**c**) $Au^{III}$. White precipitate was detected in the reactions marked with an asterisk, and correlates with a decrease in band intensity . **d**, Modelling alternative locations for placement of Cys residues on the surface of the TRAP ring, based on PDB 4V4F, and shown in orthogonal views: K35C, S33C, and D15C, with the location of the substituted residues rendered in red, cyan, and purple, respectively. **e**, Reaction of $TRAP^{S33C,R64S}$ with Au-TPPMS produces uniform cage structures, as shown by native PAGE (left) and TEM (right). Scale bar = 100 nm. **f**, Reaction of $TRAP^{D15C,R64S}$ with Au-TPPMS fails

to produce higher-order structures, as shown by native PAGE. Gels **a**-**e** and TEM were repeated independently, twice, each giving similar results. Positions of molecular weight markers on gels are indicated and arrowheads indicate position of TRAP-cage produced using Au-TPPMS. For gel source data, see Supplementary Figure 1.

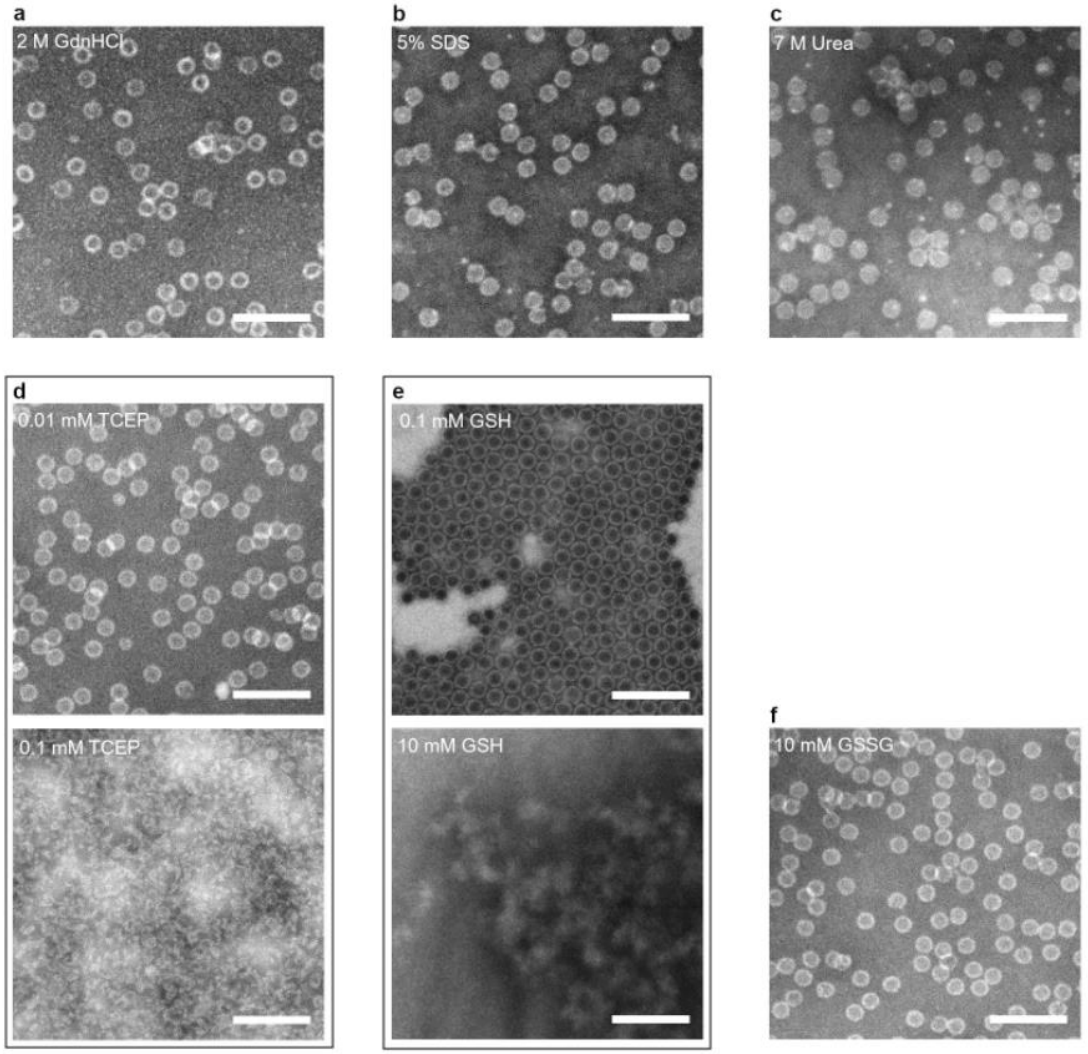


**Extended Data Figure 8. Additional tests of TRAP-cage stability.** TRAP-cage was prepared as for cages in Fig. 1d. Purified TRAP-cage samples were incubated at room temperature overnight in **a**, 2 M guanidinium-HCl, **b**, 5 % SDS, **c**, 7 M urea, **d**, 0.01 and 0.1 mM TCEP, **e**, 0.1 and 10 mM GSH, **f**, 10 mM GSSG, and subsequently imaged under TEM. All TEM images shown are representative of data that was repeated once, each giving similar results, Scale bar = 100 nm.

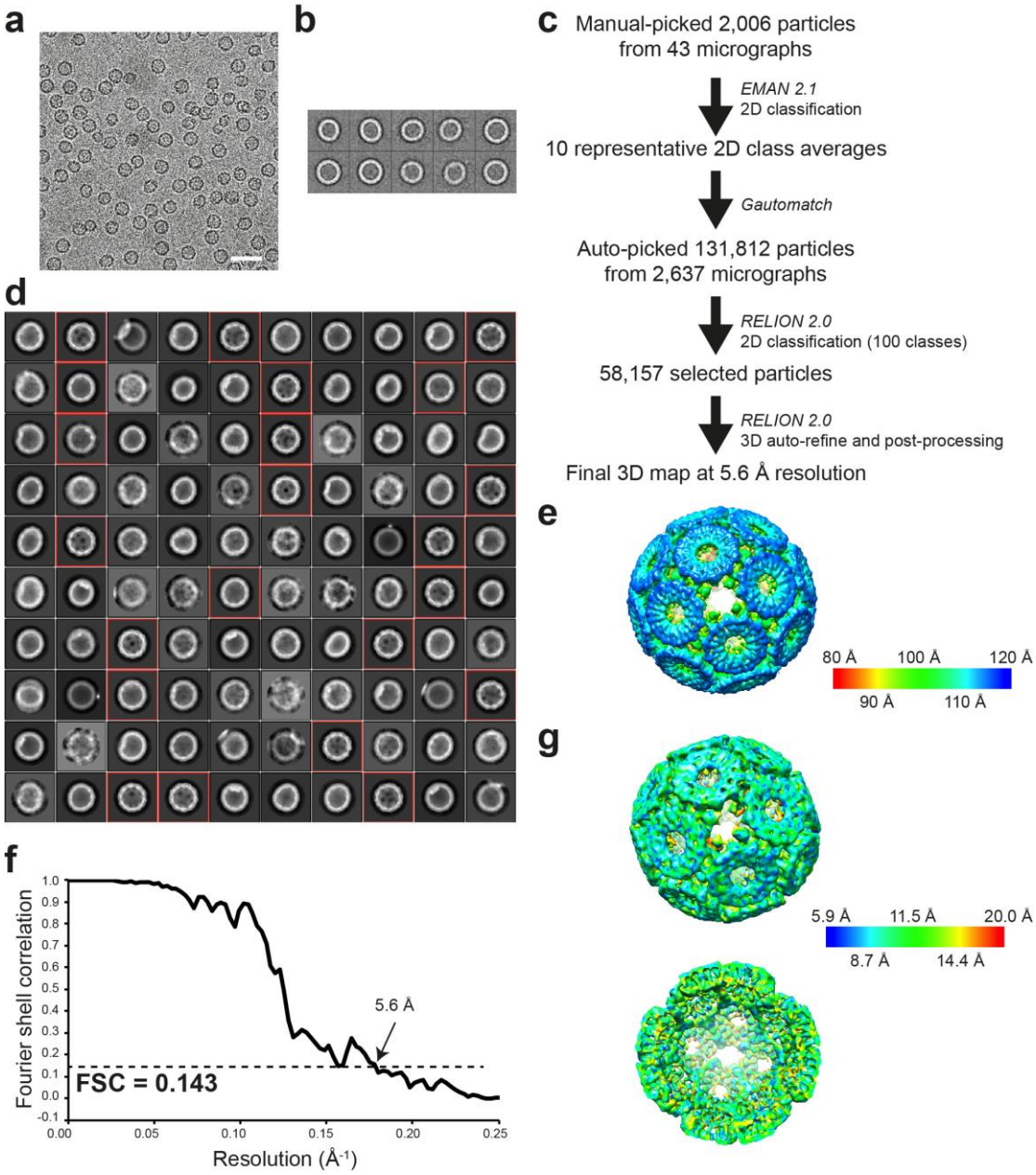


**Extended Data Figure 9. Procedure for cryo-EM single-particle reconstruction, map quality and resolution for TRAP-cage formed with GNP. a,** A representative micrograph of the TRAP-cage formed using GNP. Scale bar = 50 nm. **b,** Images of selected 2D classes from reference-free 2D classification by EMAN 2.1, used for automated particle picking with Gautomatch (box size: 220 × 220 pixels, 400.4 × 400.4 Å). **c,** Summary of the image processing procedure (see Methods). **d,** 2D class averages from reference-free 2D classification by RELION 2.0. The selected 2D class averages (22 images) for further image processing are highlighted with red squares. It is notable that in some cases (e.g. row 1 panel 9) structures

inside the TRAP-cage are visible likely reflecting stochastic capture of TRAP rings as cargo in the cage interior. **e,** Initial structure used for the high-resolution analysis. The surface representations are coloured according to the distance from the centre of the particle. **f,** Gold-standard FSC curve for the cryo-EM map from 58,157 particles. The calculated spatial frequency at 0.143 criterion was 5.6 Å. **g,** The refined density map coloured by local resolution in surface and slice views.

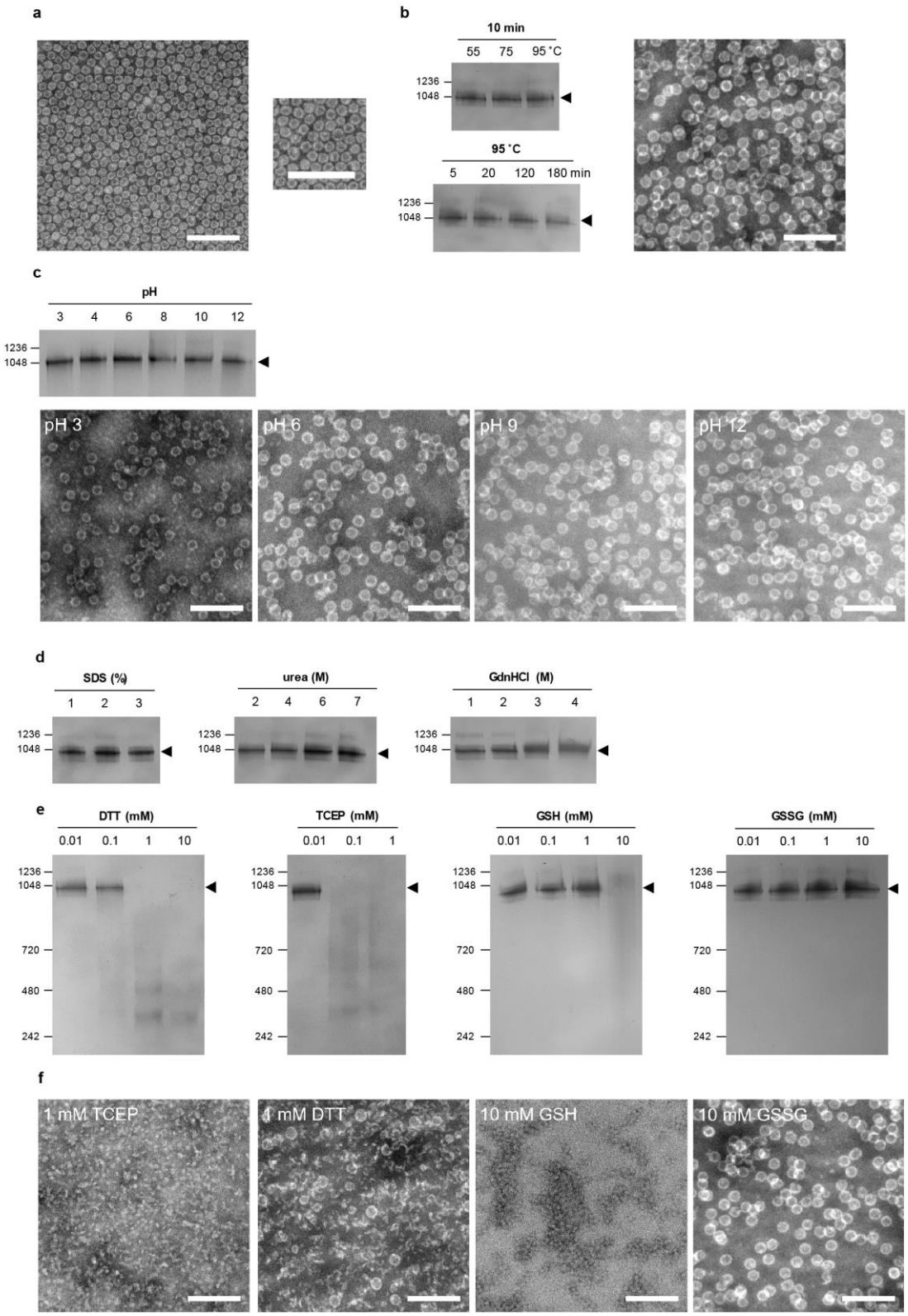


**Extended Data Figure 10. Formation and stability of TRAP-cage formed with GNPs (TRAP-cage$^{GNP}$).** TRAP-cages were formed in GNP-cage formation conditions (see Methods). **a**, TEM image of purified TRAP-cage$^{GNP}$ , with a close-up view on the right. **b**, Thermal

stability of TRAP-cage$^{GNP}$ upon incubation at the indicated temperatures and times. TEM image shows that structural integrity is maintained after incubation at 95 °C for 180 min. **c**, Stability of TRAP-cage$^{GNP}$ as a function of pH. **d,** Stability of TRAP-cage$^{GNP}$ under different chaotropic agents: SDS (1-3%), urea (2-7 M) and guanindine-HCl (1-4 M). **e-f,** Reducing agents trigger disassembly of TRAP-cage$^{GNP,}$ as shown by (**e**) native PAGE and (**f**) TEM. Assay conditions are indicated above each lane on the gel. Positions of molecular weight markers are indicated and arrowheads show position of TRAP-cage. For TEM, scale bars = 100 nm. All gels and TEM images shown are representative of experiments repeated independently at least once, each giving similar results. For gel source data, see Supplementary Figure 1.

**Extended Data References**


1 Malay, A. D., Watanabe, M., Heddle, J. G. & Tame, J. R. H. Crystal structure of unliganded TRAP: implications for dynamic allostery. *Biochem. J.* **434**, (2011).

2 Campbell, J. L., Hopman, T. L., Maxwell, J. A. & Nejedly, Z. The Guelph PIXE software package III: alternative proton database. *Nucl. Instrum. Meth. B* **170**, 193-204, (2000).

3 Simms, G. A., Padmos, J. D. & Zhang, P. Structural and electronic properties of protein/thiolate-protected gold nanocluster with "staple" motif: A XAS, L-DOS, and XPS study. *J. Chem. Phys.* **131**, 214703 (2009).

4 Zhang, P. & Sham, T. X-ray studies of the structure and electronic behavior of alkanethiolate-capped gold nanoparticles: the interplay of size and surface effects. *Phys. Rev. Lett.* **90**, 245502 (2003).

5 Movasaghi, Z., Rehman, S. & Rehman, I. U. Raman Spectroscopy of Biological Tissues. *Appl. Spectrosc. Rev.* **42**, 493-541, (2007).

| Measurements | PDI* | Mean diameter (nm)† |
|---|---|---|
| 1 | 0.074 | 21.62 |
| 2 | 0.025 | 22.51 |
| 3 | 0.050 | 22.25 |
| 4 | 0.020 | 22.25 |
| 5 | 0.020 | 22.11 |
| 6 | 0.017 | 22.23 |
| 7 | 0.044 | 23.38 |
| 8 | 0.046 | 22.48 |
| 9 | 0.042 | 22.50 |
| Mean | 0.038 | 22.26 |
| S.D. | 0.019 | 0.28 |

**Extended Data Table 1: Average size of TRAP-cage determined by dynamic light scattering.**

Results of DLS measurements based on three separate preparations of purified TRAP-cage, each measured in triplicate..

(a) PDI = Polydispersity index.

(b) Mean diameter based on volume distribution.

| | LH TRAP-cage (EMDB-4443) (PDB 6IB3) | RH TRAP-cage (EMDB-4444) (PDB 6IB4) |
|---|---|---|
| **Data collection and processing** | | |
| Magnification | 75000 | 75000 |
| Voltage (kV) | 300 | 300 |
| Electron exposure (e–/Å$^2$) | 40 | 40 |
| Defocus range (μm) | -0.9 ÷ -3.4 | -0.9 ÷ -3.4 |
| Pixel size (Å) | 0.87 | 0.87 |
| Symmetry imposed | Oh | Oh |
| Initial particle images (no.) | 10386 | 10386 |
| Final particle images (no.) | 10290 | 10290 |
| Map resolution (Å) | 3.7 | 3.7 |
| FSC threshold | 0.143 | 0.143 |
| Map resolution range (Å) | 3.0 ÷ 7.0 | 3.0 ÷ 7.0 |
| **Refinement** | | |
| Initial model used (PDB code) | 4v4f | 4v4f |
| Model resolution (Å) | 1.9 | 1.9 |
| Map sharpening *B* factor (Å$^2$) | -236 | -244 |
| Model composition | | |
| Non-hydrogen atoms | 135552 | 135552 |
| Protein residues | 17688 | 17688 |
| Ligands | 120 | 120 |
| *B* factors (Å$^2$) | | |
| Protein | 64.65 | 61.07 |
| Ligand | 219.22 | 210.12 |
| R.m.s. deviations | | |
| Bond lengths (Å) | 0.08 | 0.06 |
| Bond angles (°) | 0.656 | 0.596 |
| Validation | | |
| MolProbity score | 0.93 | 1.02 |
| Clashscore | 1.72 | 2.43 |
| Poor rotamers (%) | 0 | 0 |
| Ramachandran plot | | |
| Favored (%) | 98.04 | 98.04 |
| Allowed (%) | 1.96 | 1.96 |
| Disallowed (%) | 0 | 0 |

**Extended Data Table 2: Cryo-EM data collection, refinement and validation statistics**

| Measurement | Gold concentration (mg/ml) | SD of measurement (mg/ml) | Equivalent no. of Au per cage | SD in no. of Au per cage |
|---|---|---|---|---|
| 1 | 9.34 | 0.6 | 103 | 7 |
| 2 | 9.23 | 0.3 | 102 | 3 |
| 3 | 9.58 | 1.0 | 106 | 11 |
| 4 | 10.99 | 0.2 | 121 | 2 |
| 5 | 11.12 | 0.3 | 123 | 3 |

**Extended Data Table 3: Determination of Au content of TRAP cages using ETAAS.**Results of 5 ETAAS measurements of TRAP-cage, each performed in triplicate, showing the measured mass of gold and its translation into number of gold atoms per TRAP-

cage. Measurement 3 was discarded in calculation of overall averages due to the large observed error.

**Supplementary Information**

**Supplementary Figure:** Uncropped photographs of gels with molecular weight marker indications

**Supplementary Movies:** Supplementary movies show data obtained using single molecule mass photometry as described in the methods section. Movies 1-8 are of $TRAP^{CS}$ at various time points (30 s, 270 s, 510 s, 750 s, 990 s, 1110 s, 1230 s, and 1350 s respectively) after addition of Au-TPPMS. Movie 9 is a control of the same but in the absence of Au-TPPMS.
All scale bars are 1 µm. Each movie shows the first 0.6 s of the video only (due to size constraints on host website). Contrast is scaled to +/- 2.5 MDa. Experiments were run twice, giving similar results with representative results shown.

## Source Data

Main Fig. 1c

Extended Data Fig. 1j

Extended Data Fig. 6a